VIRUS: production and deployment of a massively replicated fiber integral field spectrograph for the upgraded Hobby-Eberly Telescope*

Gary. J. Hill[a,b†], Sarah E. Tuttle[a], Niv Drory[a], Hanshin Lee[a], Brian L. Vattiat[a], D.L. DePoy[c], J.L. Marshall[c], Andreas Kelz[d,e], Dionne Haynes[d,e], Maximilian H. Fabricius[f], Karl Gebhardt[b], Richard D. Allen[c], Heiko Anwad[l], Ralf Bender[f,g], Guillermo Blanc[h], Taylor Chonis[b], Mark E. Cornell[i], Gavin Dalton[j], John Good[a], Thomas Jahn[d,e], Herman Kriel[a], Martin Landriau[a], Phillip J. MacQueen[a], J. D. Murphy[k], Trent W. Peterson[a], Travis Prochaska[c], Harald Nicklas[l], Jason Ramsey[a], M.M. Roth[d,e], R.D. Savage[a], & Jan Snigula[f]

[a] McDonald Observatory, [b]Department of Astronomy, University of Texas at Austin, 2515 Speedway, C1402, Austin, TX 78712, USA

[c] Department of Physics and Astronomy, Texas A&M University, 4242 TAMU, College Station, TX 77843, USA

[d] Leibniz Institute for Astrophysics, An der Sternwarte 16, 14482 Potsdam, Germany

[e] innoFSPEC Potsdam, An der Sternwarte 16, 14482 Potsdam, Germany

[f] Max-Planck-Institut für Extraterrestriche-Physik, Giessenbachstrasse, D-85748 Garching b. München, Germany

[g] Universitäts-Sternwarte München, Scheinerstr. 1 , 81679 München, Germany

[h] Observatories of the Carnegie Institution for Science, 813 Santa Barbara Street, Pasadena, CA 91101, USA

[i] MIT Lincoln Laboratory, ETS Field Site, P.O. Box 1707, Socorro, NM 87801, USA

[j] Department of Physics, Oxford University, Keble Road, Oxford, OX1 3RH, UK

[k] Institute for Advanced Study, 1 Einstein Dr, Princeton, NJ 08540, USA

[l] Institut für Astrophysik Göttingen, Friedrich-Hund-Platz 1, 37077 Göttingen, Germany

ABSTRACT

The Visible Integral-field Replicable Unit Spectrograph (VIRUS) consists of a baseline build of 150 identical spectrographs (arrayed as 75 unit pairs) fed by 33,600 fibers, each 1.5 arcsec diameter, at the focus of the upgraded 10 m Hobby-Eberly Telescope (HET). VIRUS has a fixed bandpass of 350-550 nm and resolving power R~700. VIRUS is the first example of industrial-scale replication applied to optical astronomy and is capable of surveying large areas of sky, spectrally. The VIRUS concept offers significant savings of engineering effort, cost, and schedule when compared to traditional instruments.

The main motivator for VIRUS is to map the evolution of dark energy for the Hobby-Eberly Telescope Dark Energy Experiment (HETDEX‡), using 0.8M Lyman-α emitting galaxies as tracers. The full VIRUS array is due to be

* The Hobby – Eberly Telescope is operated by McDonald Observatory on behalf of the University of Texas at Austin, Pennsylvania State University, Ludwig-Maximillians-Universität München, and Georg-August-Universität, Göttingen

† G.J.H.: E-mail: hill@astro.as.utexas.edu

‡ http://hetdex.org/

Ground-based and Airborne Instrumentation for Astronomy V, edited by Suzanne K. Ramsay, Ian S. McLean, Hideki Takami, Proc. of SPIE Vol. 9147, 91470Q · © 2014 SPIE · CCC code: 0277-786X/14/$18 · doi: 10.1117/12.2056911

deployed starting at the end of 2014 and will provide a powerful new facility instrument for the HET, well suited to the survey niche of the telescope, and will open up large area surveys of the emission line universe for the first time. VIRUS is in full production, and we are about half way through. We review the production design, lessons learned in reaching volume production, and preparation for deployment of this massive instrument. We also discuss the application of the replicated spectrograph concept to next generation instrumentation on ELTs.

Keywords: Telescopes: Hobby-Eberly, Astronomical instrumentation: Spectrographs, Spectrographs: VIRUS, Spectrographs: Integral Field, Spectrographs: performance

1. INTRODUCTION: HET WIDE FIELD UPGRADE AND VIRUS

Large, targeted, spectroscopic surveys of continuum-selected objects are now becoming the norm, and have greatly increased our understanding in many areas of astronomy. Surveys of the emission-line universe, however, are limited currently to wide field imaging with narrow band filters[1], or to narrower fields with Fabry-Perot etalons or adaptations of imaging spectrographs[2]. Integral field (IF) spectrographs offer a huge gain over these techniques, depending on the application, providing greater sensitivity and wavelength coverage as well as true spectroscopy. The current generation of IF spectrographs is well-adapted to arcminute-scale fields of view, with several thousand spatial elements, and adequate spectral coverage for targeted observations of individual extended objects. They have the grasp to detect simultaneously of order 0.5 million (spectral x spatial) resolution elements.

1.1 Industrial-scale replication of VIRUS

In order to undertake large-scale surveys for emission-line objects, much greater field coverage is needed. Narrow-band imaging surveys can now cover large areas, but often require spectroscopic follow-up, and still do not probe sufficient volume to detect rare objects or to overcome cosmic variance. Wide-field IF spectroscopy is hard to achieve without a large multiplexing factor, so we have embarked on a program to produce an instrument that uses large-scale replication to create a unique astronomical facility capable of spectroscopic surveys of hundreds of square degrees of sky. The instrument is the Visible Integral-field Replicable Unit Spectrograph (VIRUS)[3-5], a simple, modular integral field spectrograph that is being replicated at least 150-fold, to provide an order of magnitude increase in grasp over any existing spectrograph, when mounted on the upgraded Hobby-Eberly Telescope (HET)[6-8]. Fig. 1 shows the upgraded HET as it will appear in approximately 12 months from now.

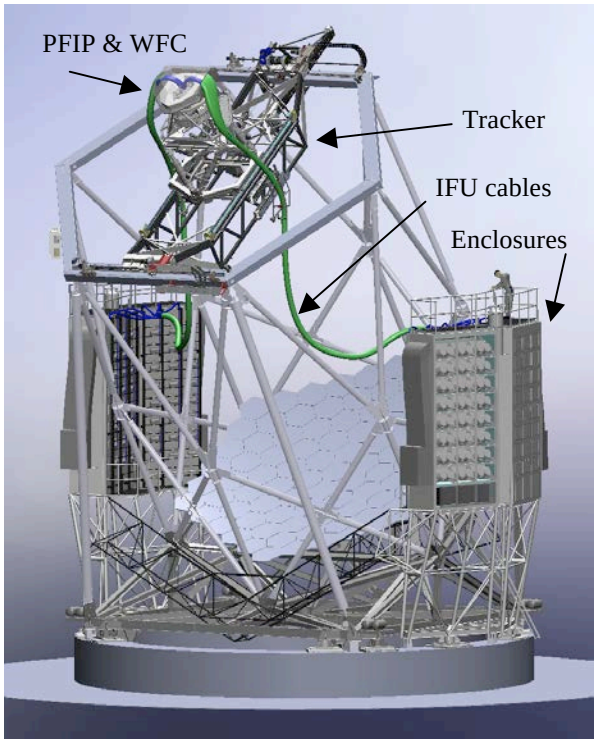

Figure 1 – Upgraded HET as it will appear in mid 2015. The new tracker supports the Wide Field Corrector (WFC) and Prime Focus Instrument Package (PFIP). The IFU fiber cables run about 20 m to the two enclosures on the VIRUS Support Structure with Cryogenic System that house the 75 to 78 pairs of integral field spectrographs that make up VIRUS.

The traditional astronomical instrument has a monolithic design and is a one-off prototype, where a large fraction of the cost is expended on engineering effort. When compared to monolithic instruments, there are cost savings from creating several copies of a spectrograph to gain multiplex advantage, because the components are less expensive and the engineering is amortized over the production run. As an example, the new MUSE[9] instrument for ESO VLT field-slices a 1 arcmin. square field into 24 duplicated IF spectrographs. VIRUS makes the next step, and exploits industrial-scale replication, which we (arbitrarily) define to be in excess of 100 spectrograph channels. We build upon the concepts laid out in Refs. 3-5, where we concluded that industrial-scale replication offers significant cost-advantages when compared to a traditional monolithic spectrograph, particularly in the cost of the optics and engineering effort.

This concept breaks new ground in optical instruments, and appears to be a cost-effective approach to outfitting the coming generation of ELTs, for certain instrument types, where the multiplex advantage of an integral field can avoid growth in the scale of instruments with telescope aperture[10].

The motivation for VIRUS is the Hobby-Eberly Telescope Dark Energy Experiment (HETDEX[11]), which will map the spatial distribution of about 0.8 million Lyα emitting galaxies (LAEs) with redshifts $1.9 < z < 3.5$ over a 420 sq. deg. area (9 Gpc^3) in the north Galactic cap and an equatorial field, using VIRUS on the upgraded HET. This dataset will constrain the expansion history of the Universe to 1% and provide significant constraints on the evolution of dark energy. The advantage of an IF spectrograph for this project is that the tracer galaxies are identified and have their redshifts determined in one observation.

The design of VIRUS flows directly from the requirements for HETDEX, to maximize the number of LAEs detected in a set observing time, and to span sufficient redshift range to survey the required volume. These science requirements flow down to the following technical requirements for VIRUS:

- Coverage of Dz ~ 2 and coverage into the ultraviolet to detect LAEs at the lowest possible redshift. VIRUS is designed for $350 < l < 550$ nm or $1.9 < z < 3.5$
- Resolution matching the linewidth of LAEs (R~700) to maximize detectability.
- Minimum throughput on sky (including atmosphere) ranging between 5% at 350 nm, 15% at 450 nm, and 10% at 550 nm to reach sensitivity of $3\text{-}4 \times 10^{-17}$ erg/cm^2/s in 20 minutes on HET.
- Low read noise detector (~3 electrons) to achieve sky-background dominated observations in 360 seconds
- High stability to ambient temperature variations, though not to gravity variations since the VIRUS modules will be fixed on HET.
- Simple, inexpensive design.

Each VIRUS unit is fed by 448 fibers that each cover 1.8 $arcsec^2$ on the sky arrayed in two spectrograph channels. The fibers feeding a two-channel unit are arrayed in a 50×50 $arcsec^2$ IFU with a 1/3 fill-factor. A dither pattern of three exposures fills in the area. The spectral resolution is 0.60 nm (R~750 at 450 nm), with coverage of 350–550 nm. The optical design is simple, using three reflective and two refractive elements. With dielectric reflective coatings optimized for the wavelength range, high throughput is obtained. The full VIRUS array will simultaneously observe a minimum of 33,600 spectra with 12 million resolution elements. In total, VIRUS has 0.7 Gpixels, comparable to the largest imagers yet deployed. The IFUs are arrayed within the 22′ field of the upgraded HET with ~1/4.5 fill factor, sufficient to detect the required density of LAEs for HETDEX. Development started with the prototype Mitchell Spectrograph (formerly VIRUS-P[4]), deployed in October 2006, and the production prototype where value engineering were used to reduce the cost for production. VIRUS is now in production, and we present here the design and lessons learned in moving from prototype to production. VIRUS is a joint project of the University of Texas at Austin (UT Austin), Leibniz-Institut für Astrophysik Potsdam (AIP), Texas A&M University (TAMU), Max-Planck-Institut für Extraterrestriche-Physik (MPE), Ludwig-Maximilians-Universität München, Pennsylvania State University, Institut für Astrophysik Göttingen, University of Oxford and Max-Planck-Institut für Astrophysik (MPA).

1.2 The Hobby-Eberly Telescope and Wide Field Upgrade

The HET[12-14] is the prototype of a new breed of cost-effective large telescopes, and is the basis for the Southern African Large Telescope (SALT)[15]. HET is an innovative telescope with an 11 m hexagonal-shaped spherical mirror made of 91 1-m hexagonal segments that sits at a fixed zenith angle of 35^o. HET can be moved in azimuth to access about 70% of the sky visible at McDonald Observatory ($\delta = -10.3^o$ to $+71.6^o$). The pupil sweeps over the primary mirror as the x-y tracker follows objects for between 50 minutes (in the south at $\delta = -10.0^o$) and 2.8 hours (in the north at $\delta = +67.2^o$). The maximum time on target per night is 5 hours and occurs at $+63^o$.

The HET was originally envisioned as a spectroscopic survey telescope, able to efficiently survey objects over wide areas of sky. While the telescope has been very successful at observing large samples of objects such as QSOs spread over the sky with surface densities of around one per 10 sq. degrees, the HET design coupled with the limited field of view of the corrector hampers programs where objects have higher sky densities. In seeking a strong niche for the HET going forward, we desire a wide field of view coupled with a highly multiplexed spectrograph in order to exploit the strengths of the telescope and of the site.

The requirement to survey large areas of sky with VIRUS plus the need to acquire wavefront sensing stars to provide full feedback on the tracker position led us to design a new corrector employing meter-scale aspheric mirrors and covering a 22-arcmin diameter field of view. The HET Wide Field Upgrade (WFU[6,7]) deploys the wide field corrector (WFC[16,17]), the new tracker[18], prime focus instrument package (PFIP[19,20]), and metrology systems[21-23]. The new corrector has improved image quality and a 10 m pupil diameter. The periphery of the field will be used for guiding and wavefront sensing to provide the necessary feedback to keep the telescope correctly aligned. The WFC will give 30 times larger observing area than the current HET corrector. The WFC is being manufactured by the University of Arizona College of Optical Sciences (OSC). Delivery is projected for the end of 2014, and is the pacing item in the WFU.

A new tracker is needed to accommodate the size and five-fold weight increase of the new PFIP. It will be a third generation evolution of the trackers for HET and SALT, and is in essence a precision six-axis stage. The tracker was developed by McDonald Observatory (MDO) and the Center for Electro-Mechanics (CEM) at the University of Texas at Austin[7,18]. Deployment started in late 2013, following removal of the previous tracker and is now complete. Mount modeling and commissioning of the tracker has started and will be complete in Fall 2014.

HET requires constant monitoring and updating of the position of its components in order to deliver good images. The WFC must be positioned to 10 μm precision in focus and X,Y, and 4.0 arcsec in tip/tilt with respect to the optical axis of the primary mirror. This axis changes constantly as the telescope tracks, following the sidereal motions of the stars. Tilts of the WFC cause comatic images. In addition, the global radius of curvature of the primary mirror can change with temperature (as it is essentially a glass veneer on a steel truss), and needs to be monitored. The segment alignment maintenance system (SAMS) maintains the positions of the 91 mirrors with respect to each other, but is less sensitive to the global radius of curvature of the surface. The feedback to maintain these alignments requires excellent metrology, which is provided by the following subsystems:

- Guide probes to monitor the position on the sky, and plate scale of the optical system, and monitor the image quality and atmospheric transparency
- Wavefront sensors (WFS) to monitor the focus and tilt of the WFC
- Distance measuring interferometer (DMI) to maintain the physical distance between the WFC and primary mirror
- Tip-tilt sensor (TTS) to monitor the tip/tilt of the WFC with respect to the optical axis of the primary mirror

The upgrade adds wavefront sensing[6,7,21-23] to HET in order to close the control loop on all axes of the system, in conjunction with the DMI and TTS adapted from the current tracker metrology system. There is redundancy built into the new metrology system in order to obtain the highest reliability. Two guide probes distributed around the periphery of the field of view provide feedback on position, rotation, and plate scale, as well as providing a record of image quality and transparency. The alignment of the corrector is monitored by the wavefront sensors as well as by the DMI and TTS. The radius of curvature of the primary mirror is monitored by the combination of focus position from the WFS with the physical measurement from the DMI and checked by the plate scale measured from the positions of guide stars on the guide probes. The SAMS edge-sensors provide a less sensitive but redundant feedback on radius of curvature as well.

Two guide probes will use small pick-off mirrors and coherent imaging fiber bundles to select guide stars from the outer annulus of the field of view. They are located ahead of the focal surface, before the large rotary shutter of VIRUS. Each will range around the focal surface on precision encoded stages, accessing a 180 degree sector. They are designed to have a small size to reduce shadowing of the focal surface, and each will have a field of view of 22.6 arcsec on a side. During setup on a new target, they will be driven to pre-defined positions, and the initial pointing will be made by centering the guide stars in the probes. This system is a significant upgrade from the current pellicle-based guiders.

Two Shack-Hartmann (S-H) wavefront sensors will also range in the outer field. Their function is to provide feedback on the low-order errors in the wavefront (focus, coma, spherical, and astigmatism)[21-23]. These errors are caused by misalignment of the corrector with the primary mirror focal surface and by global radius of curvature and astigmatism errors in the primary mirror shape. Updates will be generated approximately once per minute. In addition to the WFS probes there will be an analysis wavefront sensor as part of the acquisition camera that will allow more detailed feedback analysis of the image quality, simultaneous with the operation of the WFS probes, independent of seeing. Simulations show that a S-H system with 7x7 sub-apertures across the pupil can meet the requirements using 18th magnitude stars. We previously deployed a wavefront sensor on the HET with 19 sub-apertures across the pupil and

the final design was informed by direct experience with that sensor. The PFIP includes an analysis WFS similar to this prototype, which provides the reference for telescope focus.

At the time of writing, we are half way through the installation of the WFU. The new tracker is installed and is functional, making moves and tracks under the telescope control system. The WFC is still ~6 months from delivery due to problems at UA OSC. In the meantime, we will be installing the enclosures and cryogenic system for VIRUS and developing the mount models for the telescope so as to be ready to go on-sky as soon as possible following delivery of the WFC.

3. THE VIRUS PROTOTYPE: MITCHELL SPECTROGRAPH (VIRUS-P)

The motivation for building the VIRUS prototype (Mitchell Spectrograph, formerly VIRUS-P[4]) was to provide an end-to-end test of the concepts behind HETDEX, both instrumental and scientific. Construction and testing of the prototype have verified the opto-mechanical design, the throughput, the sensitivity, and demonstrated the utility of such an instrument for surveys of emission-line objects. It has also served as a test-bed for the software development needed for analyzing the data from the full VIRUS array. The parallel nature of VIRUS means that the prototype can be used to develop the final software pipeline. The Mitchell Spectrograph was also designed to be a facility instrument on the McDonald 2.7 m Smith Telescope (HJST). On the HJST at f/3.65, the 200 μm fiber cores subtend 4.1 arcsec, and the IFU covers 3.5 arcmin^2. While the fibers are large, projected on the sky, the IFU covers the largest area of any current IF spectrograph and this results in great sensitivity for wide area surveys and particularly for spatially extended low surface brightness emission[24]. Other science applications have included high redshift galaxies[25], and studies of resolved nearby galaxies[26,27].

The Mitchell Spectrograph has been used for a pilot survey of Ly-α emitting galaxies in support of the HETDEX project (HPS, Refs 38-40). The survey covers 166.4 arcmin^2 on the COSMOS, MUNICS-S2, and GOODS-N fields and detects 107 LAEs and 368 low redshift emitters[28]. The results of the HPS confirm the sensitivity estimates on which HETDEX is based[29], and demonstrate the effectiveness of blind IFU spectroscopy for this application. The HPS sample is unique in the volume it probes, when compared to narrow band searches which reach deeper but are highly influenced by cosmic variance, and includes a significant number of luminous LAEs which have allowed follow up in the near infrared to study rest-frame optical emission lines of H-α, H-β, and [OIII] yielding interesting results on the metallicities of these objects[30,31].

The VIRUS instrument consists of three basic sub-units: the IFU, the collimator/grating assembly, and the camera assembly. The beam size is 125 mm, allowing the collimator to accept an f/3.32 beam from the fibers, accommodating a small amount of focal ratio degradation of the f/3.65 input from the telescope. The camera is a f/1.33 vacuum Schmidt design with a 2k x 2k format CCD with 15 μm pixels at its internal focus.

Detailed discussion of the Mitchell Spectrograph is presented in Ref. 4, here we summarize the results:

- Throughput of the Mitchell Spectrograph as a function of wavelength (ignoring aperture effects at the input to the fibers) peaks at 40% with 15 m long fibers, in line with predictions based on the measured throughputs of individual components. On-sky at the HJST, including the atmosphere, the throughput peaks at 18%. This performance meets or exceeds that required for HETDEX, when projected HET throughput is considered, except at the very shortest wavelengths.
- The 5-σ point source line flux sensitivity is ~5x10^{-17} erg/cm^2/s, in 2 hours observing, in line with predictions. The number of emission-line galaxies detected in the HPS are in line with predictions, confirming the models on which HETDEX predictions are based.
- Image quality of the instrument meets requirements. Optical alignment was achieved with simple setup procedures.
- The instrument is extremely stable against temperature changes, with images moving 1/20 of a resolution element with a 12 Celsius temperature change, exceeding requirements. On HET, the VIRUS units will be mounted fixed, so stability against gravity vector changes is not a requirement.

4. VIRUS PRODUCTION DESIGN

Evolution of the design of VIRUS from the prototype to the production model was made in two steps. First a pre-production prototype was developed that incorporated the production engineering to reduce costs. In particular

aluminum and Invar castings for components including the cryostat were prototyped and qualified. Second, small design modifications gleaned from this experience were incorporated into the First Article production unit and that was followed by production of an initial batch of 3 units which became references for production of IFUs, collimators and cameras in different locations[5].

VIRUS naturally splits into three major subsystems (IFU, collimator, and camera), which have kinematic interfaces between them. Cameras are being produced at UT Austin[32], collimators at TAMU[33], and IFUs at AIP[34]. Oxford University provided a large number of mechanical parts for the collimators and cameras, and IAG has manufactured many IFU components and the input head mount plate that mounts them to the telescope. Spectrograph integration, alignment, and characterization is led by UT Austin. Full spectrograph production started in 2013 and at the time of writing we are about ½ way through.

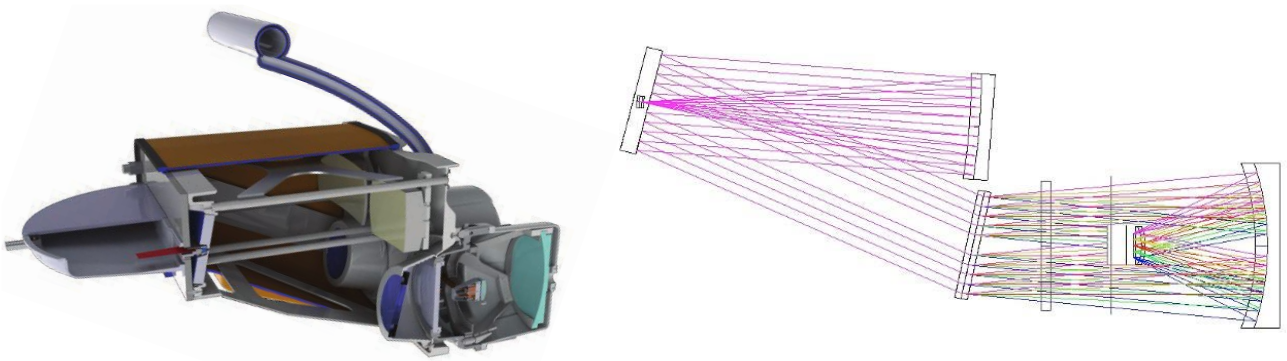

Figure 2: Layout of the production VIRUS. Left shows the production mechanical design and right shows the optical design. The grating has 930 l/mm and the coverage is fixed at 350-550 nm. The mechanical cutaway shows the IFU slit assembly on the left, mounted to the collimator. The Schmidt camera has an internal CCD in the vacuum and mounts to the main bulkhead of the collimator. It is cooled by a flexible line from above with a breakable cryogenic bayonet connection.

4.1 VIRUS Production Optomechanical Design

While the VIRUS units are mounted in fixed housings, their enclosures track ambient temperature and they are required to operate with high stability under a wide range of temperature from -5 to +25 degrees Celsius. The instrument is specified to not require recalibrating for shifts in the positions of the fiber spectra over the temperature range encountered in an hour, with the goal of maintaining alignment during an entire night. Stability is crucial since the data reduction and analysis is sensitive to 0.1 pixel shifts in the spectra. This requirement corresponds to shifts smaller than 0.5 pixels (1/10 of a resolution element) at the detector for 5 degrees Celsius temperature change. The Mitchell Spectrograph was designed to test this requirement. It is mounted in a gimbal to maintain its orientation, but sees the full temperature swing in a night.

For production, we made some significant changes to the design, based on experience with the Mitchell Spectrograph and responding to the development for the HET WFU design. The most significant was to double the spectrographs so that a pair shares a single IFU, a common collimator housing, and a common cryostat (Fig. 2). The motivation for this came first from fiber cable handling: it is more efficient in terms of weight and cross-sectional area to double the number of fibers in a cable (note that the fiber itself is not the dominant weight in a bundle). There is not a significant cost-savings on the IFU, since the majority of the cost is in the fiber, but volume occupied by the cables is reduced and the cable handling becomes significantly easier with 75 instead of 150 cables to accommodate (the goal is 78 cables, and the IFU handling system is being designed with enough capacity). The other advantage to the double unit is that two cameras share a vacuum, and have a single connection to the liquid nitrogen (LN) cooling system. This increases the evacuated volume in an individual cryostat, which increases hold-time, and saves cost on vacuum valves and other fixturing. Pairing the spectrographs enabled reduction of mechanical structure to support optics by eliminating the redundant structure of two spectrographs placed side-by-side. The complexity of the enclosures to house the spectrographs was also reduced by pairing the instruments because fewer interfacial features between instrument and superstructure are required.

The optical layout has been modified to make the system more linear and allow the units to be packed more tightly in the housings (Fig. 2). Analysis of the fiber diameter for maximizing the number of Lyman-α emitting (LAE) galaxies detected by the HETDEX survey indicates that the ideal is 1.5 arcsec for the expected range of image quality to be encountered in the survey (1.3 to 1.8 arcsec FWHM). Analysis of the expected number of LAEs with redshift also indicates that the majority of the objects are located at $z<3.5$ due to the change in distance modulus with redshift coupled with the steepness of the LAE luminosity function. As a result, the decision has been made to reduce the wavelength coverage so as to preserve spectral resolution, while accommodating the larger fibers (266 vs 200 μm core diameter). This is a small change and the increase in dispersion of the grating (930 versus 830 l/mm used for the HPS) does not effect diffraction efficiency over the observed bandpass. Wavelength coverage is 350 – 550 nm ($1.9 < z < 3.5$) and resolving power is R=700 at 450 nm.

Figure 3 shows an exploded view of the spectrograph unit. The VIRUS optics and mechanical interfaces were carefully specified to produce optics that will be interchangeable amongst any VIRUS unit. Both the optical and mechanical properties of each optic have been carefully toleranced using Monte Carlo realizations of the collimator and camera that were then combined and evaluated. The optical tolerancing is described in detail in Ref 35. Particular attention was paid to the relative alignment of the axes of the two spectrographs within a single unit.

Detailed information on the VIRUS mechanical design is given in Refs 36-39. Relatively early in the production mechanical design of VIRUS we investigated castings for large aluminum bulkhead parts. Castings offer the potential to produce part shapes that might otherwise be impossible or prohibitively expensive to machine from a solid billet of material. As a result, they offer the designer structures that can be exceedingly lightweight and stiff. However, casting is often characterized by its lack of precision and repeatability, which does not lend itself well to producing instrumentation. In addition, casting processes traditionally require high up-front costs for fabricating the molds making them uneconomical for low-quantity production and risky for design efforts where prototyping is required. We adapted our design to these factors, and the recent proliferation of stereo lithography and other rapid prototyping devices has significantly decreased the cost of producing prototype castings. Complex part shapes are quickly and economically "3D printed" using stereo lithography equipment or machined from plastic foam. Those parts can then be used to imprint sand molds or in the case of investment casting, coated with refractory material and melted out through a sprue. Several companies offer fast turnaround, low cost prototype casting services and can accept CAD models online without need for mechanical drawings. As a result, we were able to prototype subassemblies with castings without incurring prohibitive costs, and were able to gain an understanding of the design principles needed in using castings.

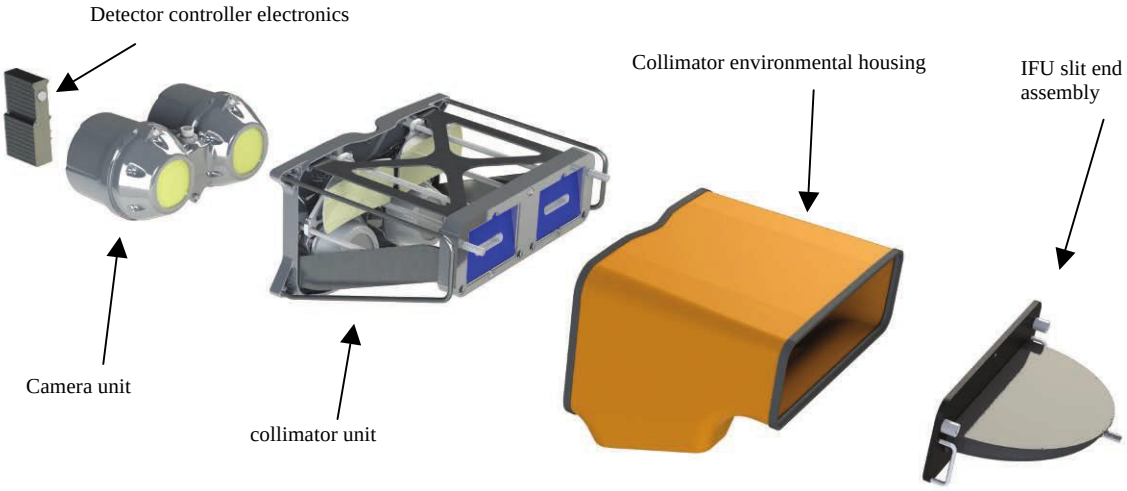

Figure 3. Basic components of the VIRUS unit housing two spectrographs. Light enters at the IFU slit assembly along two axes. The collimator holds the IFU and camera cryostat on kinematic mounts and forms the main structure of the instrument. The cameras are interchangeable and removable should maintenance be required. The detector controllers mount directly to the cryostats.

In the final design, we adopted cast aluminum cryostats and grating housings and cast Invar detector supports. Prototyping of aluminum castings for the major bulkheads in the collimator demonstrated that the part-to-part variation (due primarily to warping of the cast parts) required significant labor in setting the parts up for post-machining. We were able to prove the concept and produced collimator structures within specification, but in the end we adopted bulkheads machined from large billets of aluminum jig stock. This represented the cheaper alternative for the Oxford Physics machine shop due to high labor costs coupled with large CNC mill capacity. They adopted a production sequence that involved very low labor to set up and machine several bulkheads at once.

Kinematic mounts enable highly repeatable registration between components and their use is prevalent in precision optical assemblies. The VIRUS spectrograph relies on kinematic mounts between sub-assemblies, which are considered modular to each other, specifically the IFU slit assembly, the collimator, and the camera. The optical and mechanical tolerances of the instrument are arranged such that modules of a particular type would be interchangeable. For example, the camera couples to the collimator through a kinematic mount. Originally it was required that any camera could be used with any collimator and perform within specification. However, experience in alignment led us to instead allow both camera and collimator mirrors to be adjusted, leading to better than specification image quality at the expense of making the camera and collimator matched for a given spectrograph unit (see Sec. 6 for details). Similarly, the VPH gratings are modular to the collimator and the detector sub-assemblies are modular to the camera body.

4.2 Collimators and Gratings

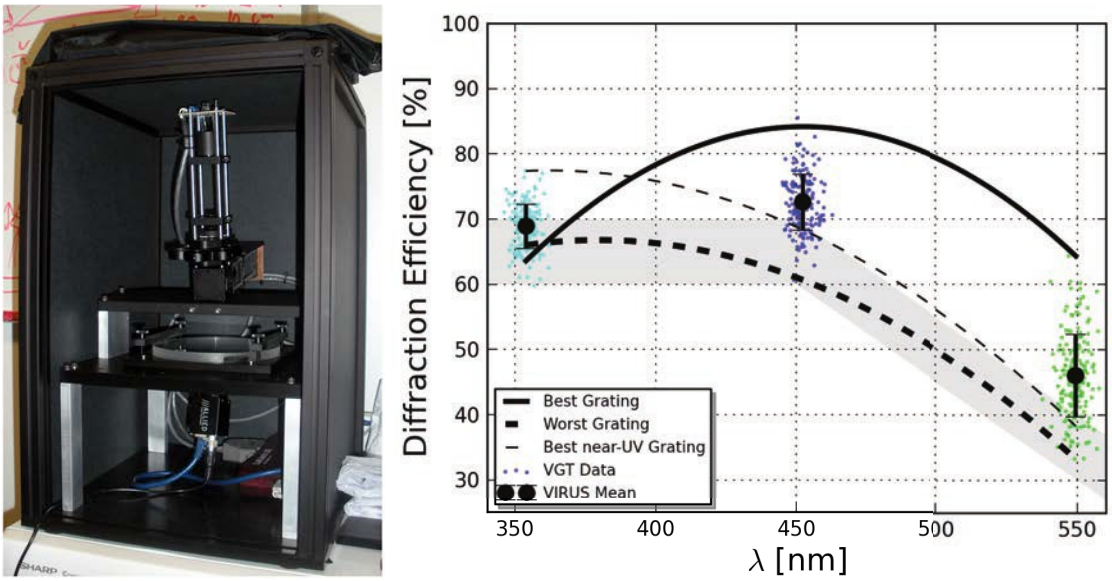

Figure 4. Left shows the grating tester supplied to SyZyGy to provide absolute efficiency and scattering measurements during production. Right shows the results of external diffraction efficiency testing of 170 gratings at three wavelengths compared to the requirements. The shaded region shows the required minimum bound and mean for the diffraction efficiency at the three test wavelengths. The solid black line shows the best overall grating, based on integrated area under the efficiency curve, and the light dashed line the grating with the best UV efficiency. The heavy dashed curve is the worst accepted grating.

Collimators and gratings (Figures 4,5) are assembled efficiently at TAMU, mainly using student labor from parts supplied by Oxford, UT, and TAMU[33]. The fold flats are integrated into the front bulkhead with a simple centering grid and glued in place with epoxy. Assembly of the mechanical structure takes on the order of an hour. A Faro CMM arm is used for alignment of the optics to within 100 μm tolerance. The gratings are glued into their cells and set for rotation in their housings. At the time of writing, 61 production collimator units are assembled (Fig. 5). They are shipped to UT Austin as needed for integration with cameras.

VIRUS uses volume phase holographic (VPH) gratings, which offer high efficiency and low cost. The setup for HETDEX employs VPH gratings with physical dimensions of 148 mm in diameter by 16 mm in total thickness; the VPH layer itself has a 138 mm diameter clear aperture and is sandwiched between two 8 mm thick, anti-reflection (AR)

coated fused silica substrates using an optical grade adhesive. The grating has a fringe frequency of 930 lines/mm and operates at order m = 1 in transmission from 350 to 550 nm for unpolarized light. Efficiency is optimized for the UV by lowering the angle of incidence away from the Bragg angle, which is close to 12 degrees.

Details of the grating design, development, and testing are reported in Refs. 39-41. We undertook tests of small and full size gratings from Wasatch Photonics, Kaiser Optical Systems International (KOSI), and SyZyGy using a custom automated test-bench that can fully characterize a grating over a range of input and output angles[39]. This test bench was used to evaluate test gratings as it allows orders m=-1,0,1,2 to be measured to account for as much of the diffracted light as possible[40]. Performance in the ultraviolet was enhanced by reducing the angle of incidence to shift the blaze to the UV. Angle changes of the grating at fixed collimator angle have little effect on the wavelength range, so tilting the grating provides an independent free parameter in tuning the throughput as a function of wavelength. In addition, we specified a 1 deg. tilt of the fringes in the grating, to ensure that the "Litterow" recombination ghost[42] is off the detector for the VIRUS configuration.

In order to ensure a standardized reference for measurements of diffraction efficiency of production gratings compared to specifications, and to facilitate more rapid testing than possible with the flexible test bench mentioned above, we developed a simple rugged grating tester for the specific gratings we are procuring for VIRUS[41]. The tester is shown in Fig. 4. LEDs with wavelengths of 350,450, and 550 nm illuminate 12.5 mm subaperture on the grating surface. A silicon photodiode fed by a beamsplitter normalizes the light output of the LEDs. The angles of incidence and diffraction are fixed to the VIRUS configuration and the light is imaged onto a 2/3 format commercial CCD camera by an off-the-shelf aspheric lens. Calibration is provided by a fiducial grating that underwent a deteailed characterization on our main grating test bench. Custom software and control allow a grating to be tested in 10 minutes, including efficiency and scattered light. The position of the grating was moved laterally to sample 9 subapertures in order to provide an average efficiency more representative than spot measurements. We have found that VPH gratings exhibit quite significant small-scale variations in efficiency and it is possible to find and report a "hot-spot" in the diffraction efficiency, if too small an area is measured. This is particularly the case with laser measurements employed by some vendors. The grating tester was tailored to the properties we care about in the specification and avoided conflicts over inconsistent measurement methods between vendor and our lab.

The contract for 170 gratings was awarded by TAMU to SyZyGy and production results as gathered by the grating tester are reported in Ref. 41. Since the overall performance of the suite of gratings is of importance for VIRUS, we established requirements based on mean values for efficiency at the three test wavelengths as well as minimum requirements. Figure 4 shows the external grating diffraction efficiency, averaged over 9 sub-apertures, plotted for all 170 accepted gratings, as well as the requirements and examples of specific gratings. The production clearly exceeded requirements by a substantial margin. Gratings were integrated into cast aluminum housings that incorporate a rotational adjustment that is pre-set and then adjusted during final alignment[33].

Figure 5. Twelve completed collimators arrayed on the assembly line at TAMU

4.3 Cameras and Detector System

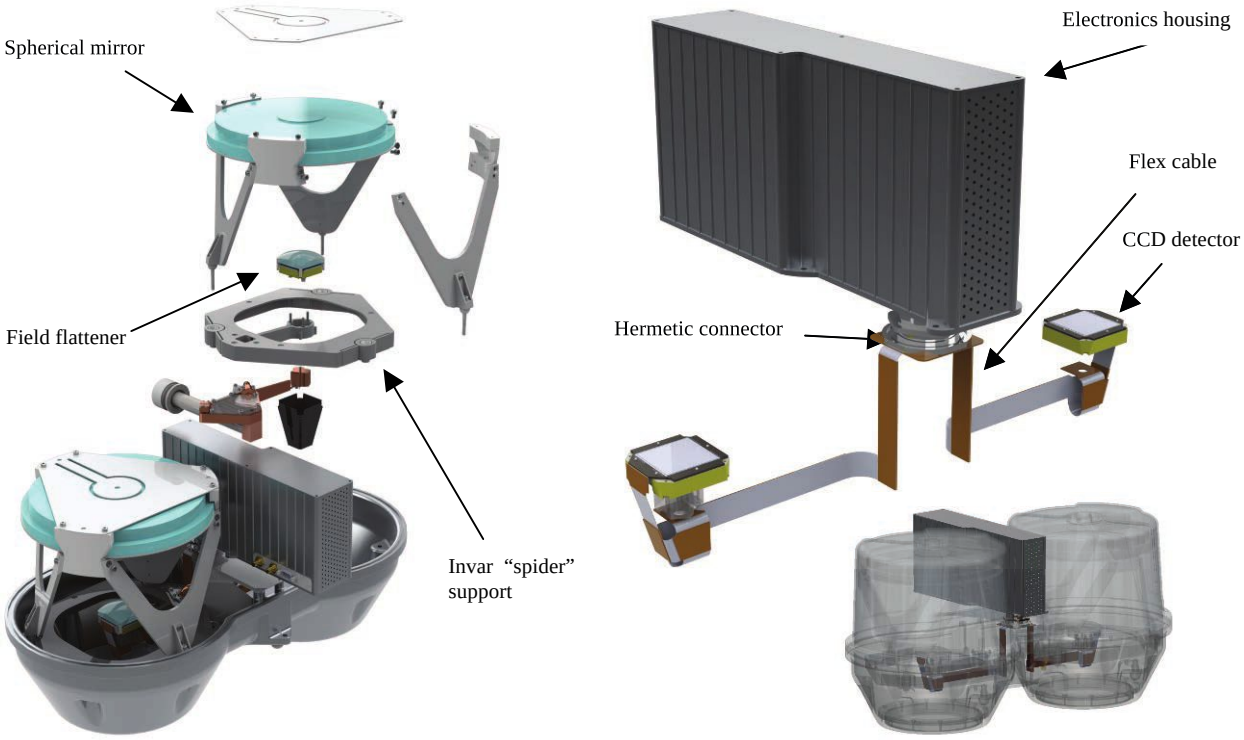

Figure 6. Camera assembly and electronics. Left shows the integration of the two camera channels into the cryostat. Right shows the detector system controller, the flex circuit, and the CCD packages as they integrate into the cryostat.

The camera cryostat vacuum is shared between a pair of spectrographs. This modification effectively halves the number of ancillary vacuum components such as valves and vacuum gauges. This saves not only the expense of these components but reduces the number of sealing surfaces that contribute to long-term vacuum degradation and are a point of failure. The larger evacuated volume also leads to longer vacuum hold-time. Similarly, the cryogenic cooling system is shared within a unit. This reduces the part-count of the instrument cryogenic system and also simplifies the cryogenic distribution system and losses associated with fittings and valves. The cryogenic system development and testing is described in greater detail in Sec. 7 and Refs. 43,44. The cryostat is composed of two aluminum castings, post-machined only on critical mount surfaces and flanges. Cryostats were manufactured by MKS Inc., following extensive evaluation of prototypes. An impregnating step with Locktite Resinol, following machining, ensures that the porosity of the cast aluminum does not lead to virtual leaks or poor vacuum seals, and leak rates are achieved that are consistent with the O-ring length and internal volume of the cryostat. While the tooling cost for casting is quite significant, the cost for even a single cryostat of this size is competitive with machining from bulk stock, and is much cheaper for the VIRUS production run. Cryostats are all delivered and production is discussed in Ref. 32.

The stability of the instrument to temperature changes is crucial, as discussed above. While the Mitchell Spectrograph design was very successful in this regard, we traced the small residual instability with ambient temperature swings to movement of the camera mirror. In VIRUS the detector head assembly is all Invar with a cast "spider" mounting the detector and field flattener and an Invar truss structure supporting the mirror (Figs. 6,7).

The CCDs for VIRUS have a nominal 2kx2k format with 15 μm pixels. The required readout time is relatively slow at 20 seconds, binned 2x1, but low read noise (~3 electrons) is required and the parallel readout of up to 156 CCDs is still challenging. The VIRUS system is 630 Mpixel, which is comparable to MUSE[45] and to the largest imaging mosaics yet deployed. The data volume from the full VIRUS array is about 2.5 GB per observation. Observation times per field are 20 minutes for the HETDEX survey, split into three exposures, and we expect to generate 40 TB of raw

data over the course of the survey, including calibrations. The data reduction pipeline Cure[46,47] operating in the Astro-WISE environment will reduce each night's data within 8 hours on a dedicated computer cluster at MPE.

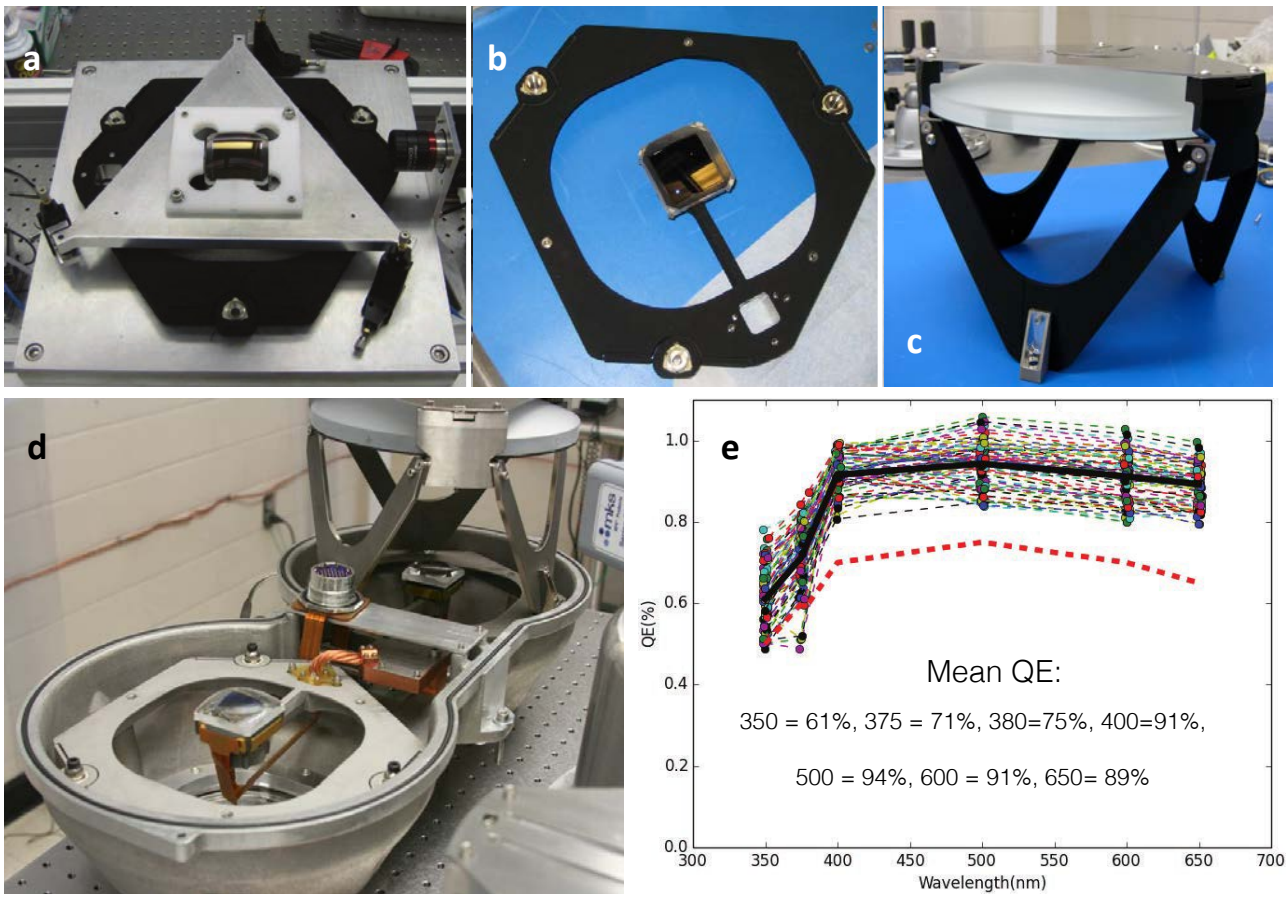

Figure 7. VIRUS camera production and detector performance. (a) alignment of field flattener lens to CCD detetector in custom jig; (b) assembled "spider" with detector and field flattener; (c) completed cameral mirror assembly ready for integration; (d) integration of cryostat (not fully metal finished first article); (e) statistics on quantum efficiency (QE) of delivered detectors – red dashed line is requirements, solid black line is mean of the batch.

In writing the specifications for the detector system, we developed metrics applied to batches of CCDs to obtain the required final science performance on average. This approach is important in keeping costs low because restrictive requirements reduce yield and increase risk and price. A good example of how we approached this is the metric for QE and read noise, which is based on S/N ratio for the expected signal level from the sky for VIRUS observations. The metric is calculated for the average of a batch of detectors, along with a minimum QE threshold as a function of wavelength and a maximum read noise threshold for any CCD. This approach allows the vendor to balance poorer read noise with increased QE and vice versa and provides greater latitude for accepting CCDs without impacting the performance we care about. The resultant increased yield provides the vendor with greater security of predicting yields and hence provides the best price. The other key specifications are very low cross-talk between the pair of CCDs in each cryostat, and between cryostats, and very low external noise pickup. Since we are searching for detections that are very few correlated resolution elements, we need to understand the noise characteristics of the data extremely well.

The integrated detector system is being provided by Astronomical Research Cameras, Inc., with the University of Arizona Imaging Technology Laboratory providing thinned backside illuminated CCDs with AR coatings optimized for the VIRUS bandpass, as a subcontract from wafers manufactured by Semiconductor Technology Associates, Inc. Since the CCDs come from custom wafer runs, we elected to increase the imaging area to 2064 by 2064 pixels, allowing more

latitude for alignment. Figure 7(e) shows the QE of delivered detectors, which exceeds the specifications comfortably, especially at the longer wavelengths. The average read noise of the 166 detectors so far delivered is 3.37 electrons[32].

The design of the detector package, flex circuit, and controller have been highly customized to the VIRUS application, since the engineering is spread over a large production run. This allowed us to remove most of the complexity associated with the detector head of the Mitchell Spectrograph[48]. Figures 6 and 7 show the layout for a pair of detectors in a single cryostat. The CCD package, machined from Invar-36, is designed for minimum obstruction and hides in the shadow of the field flattener (FF) lens. The CCDs are flat to within +/-10 μm, which is allowed by the tolerance analysis. The package has a custom header board that brings the traces to a single connector on one side of the package. A custom flex circuit with complex geometry connects the two detectors to a single 55-pin hermetic bulkhead connector (Fig. 6). The controller mounts directly to this connector, without cables, and its form-factor has been customized to fit between the cylinders of the cryostat cover.

The detector package also mounts the FF lens on four Invar flexure clips that set the separation and alignment of the FF to the detector plane (Fig. 7). Metrology of each detector is used to control these dimensions when the clips are glued to the field flattener, with the glue-line acting to take up any misalignment. The alignment jig incorporates a laser to establish the axis of the detector head, an imaging camera to view fiducial marks on the detector, and allows the field flattener to be aligned using the interference pattern generated by its front and back surfaces. Tests show this scheme has 10 μm sensitivity to tilts and decenter, within the required tolerance. Once the FF lens is installed its optical axis defines the axis of the head and allows alignment of the mounts on the "spider" that interface with machined features within the camera cryostat. Since the camera mirror structure mounts to the same points, the entire camera becomes a unit with only the aspheric corrector plate (with much lower alignment tolerances) separate.

The detector package with attached FF is then integrated into the "spider" which supports the detector head, cantilevered in the beam. The spider is of post-machined cast Invar-36 (Fig. 7), and its production is discussed further in Refs. 32,49. The whole spider is adjusted in all degrees of freedom in an alignment jig to position the FF on the axis of a laser that defines the camera axis. Four lugs are then glued in place to capture the alignment, and they interface to machined features in the cryostat housing. In this way, the alignment of the CCD and FF to the axis of the camera is achieved within the required tolerances of 50 μm in centration and separation, and 0.05 degrees in tilt[32,49].

The shutter for the system is located in front of the IFU inputs, just below the focal surface in the PFIP[19,20]. It has a rotary blade design, and a minimum exposure time of 1 second. The shutter is located remotely from the detector controllers and is commanded separately. Exposures are coordinated via the Telescope Control System, which sends simultaneous shutter-open commands to the shutter control system and to the VIRUS Data Acquisition System (VDAS) that controls the detector system. Timing between the shutter and the VDAS is maintained with a Network Time Protocol server, synchronized to GPS time.

The CCD controllers have DC power in and fiber-optic data lines out. To minimize crosstalk, the timing of all CCD clocks is synchronized to a master clock signal distributed over a Low-Voltage Differential Signal (LVDS) system. The data system requires several levels of multiplexing. First, each CCD controller commands two detectors, each with possibly two readout amplifiers. Next, a custom-built 8-way multiplexer combines the output from each set of 8 CCD controllers. Next, the output of each of 12 multplexers is fed into a PCI interface card. Two PCI-to-PCIe expansion chassis are used to connect 6 PCI interface cards each to a PCIe port in the VDAS computer. Finally, the data are transferred via DMA from the PCI interface cards into the VDAS memory. From there, the data are passed to a Cure "QuickLook" pipeline, and also written to disk as separate FITS files, one for each amplifier, to aid parallel processing of the pixels in an on-site array of CPUs. The QuickLook pipeline includes many of the algorithms developed for the full reduction of the VIRUS dataset[47], but is focused on monitoring detector health and data quality, to inform the observer of problems, and when to terminate observations due to poor conditions. In the lab we use a version of the software dubbed "LabCure" that runs scripts customized to the reporting requirements of the IFUs and full spectrographs. Lab testing has verified very low cross-talk between CCDs in the same cryostat and between multiple cameras, utilizing the full structure of the detector readout system[32].

4.4 Integral field unit cables

It is essential to couple VIRUS to the HET with fibers due to the weight and space constraints at the prime focus of the telescope. In addition, the variable effects of the changing pupil illumination of HET during a track are mostly removed by azimuthal scrambling within a fiber, producing much greater stability in the data calibration than is possible with an

imaging spectrograph. Fiber IFUs can utilize microlens arrays, providing close to 100% fill-factor[50], or be of the simpler "densepak" type[51]. For VIRUS we have elected to use the densepak type of bare fiber bundle to maximize throughput and minimize cost[52,34]. The primary advantage of lenslets is in coupling the slower f/ratios of typical foci to the fast ratio required to minimize focal ratio degradation (FRD[53-55]), and such IFUs are ideal for retro-fitting existing spectrographs. Lenslets do not provide perfect images, however, so if there is flexibility to choose the input f/ratio to the fibers and if the fill-factor can be tolerated, trading it against total area, the bare bundle provides the best efficiency[3]. Also, the central obstruction of the telescope is preserved at the fiber output to large extent if there is low FRD. This is an advantage for a catadioptric camera as in VIRUS. For the VIRUS IFUs we use a fill factor of 1/3 for the fiber cores, with the fibers in a hexagonal close pack, and dither the IFU arrays through three positions to fill the area. Note that if the f/ratio of the microlens-coupled case is the same as the f/ratio from the telescope in the bare-fiber case, and the lenslets subtend the same area on the sky as the bare fibersat that f/ratio, then the fill-factor of the densepak type array is exactly offset by the larger area that the bundle covers per exposure. So in the case where maximum areal coverage is required, and especially with an obstructed catadioptric camera, the bare bundle is the preferred solution.

The HET site has a median seeing of 1.0 arcsec FWHM, and the upgraded HET is expected to deliver 1.3 arcsec images on average. Analysis of the trade-off between areal coverage and sensitivity shows that larger fibers are preferred for HETDEX to maximize the number of detected LAE galaxies. As a result, 1.5 arcsec (266 μm) diameter fiber cores were adopted for the production VIRUS units. The WFC delivers f/3.65. The optics of VIRUS can accommodate an f/ratio of f/3.32 (within the 125 mm pupil size), allowing some focal ratio degradation and accommodation of alignment errors in the subsystems.

IFU development at the Leibniz Institute for Astrophysics (AIP)[52,34] and University of Texas at Austin (UT)[54,55] has focused on establishing a design that minimizes FRD, maximizes throughput, and is manufacturable in quantity[34]. Careful and rigorous apportioning of tolerances between the components aims to keep 95% of the transmitted light within the spectrograph pupil. Development of the prototype IFUs explored ways of setting up the required matrix of fibers at the input end. Setting up a matrix of fused silica capillary tubes to set the spacing proved very successful, but time-consuming to set up. The alternative, adopted for production, is to use micro-drilled alloy blocks to locate the fibers at the input. Anti-reflection coated fused silica cover lenses are bonded (immersed) to the polished surface of each IFU with index-matching UV curing couplant to minimize insertion losses. A mask covers the polished metal border of the head to cut down on stray light. Measurements of FRD and throughput before and after immersing the ends demonstrate marked improvement for many fibers, and results in very uniform throughput between fibers[34]. At the output of the bundle, the fibers are arrayed in a line, immersed against the curved back face of a cylindrical lens, and fanned out with their axes pointing perpendicular to the collimator mirror (and to the lens). This layout allows collimation of the beam to be achieved with only one spherical mirror, leading to a very efficient design. The corrector plate that is the window to the camera cryostat corrects both camera and collimator. The spacing between fibers is achieved by bonding the fibers to a monolithic groove plate of stainless steel.

Figure 8 shows images of the slit and input ends of production fiber cables. They each contain 448 fibers with 266 μm cores, and we have kept the design as simple and lightweight as possible. The input head consists of a precision micro-drilled block from Euro Micron into which the fibers are fed which is in turn clamped within a stainless steel shell that provides the mounting features. The fibers are glued in with epoxy and then cut off and polished. At the exit, the cable bifurcates within a slit housing into two slits with the fibers glued to grooved blocks of the same design as for the Mitchell Spectrograph. Input and output are bonded to a thin lens and a cylindrical lens, respectively, both of fused silica and AR coated. The lens on the input ensures the chief ray of the curved focal surface is normal to the fiber input for all the fibers, even though the input face is flat.

The physical design of the cables has benefitted greatly from the use of prototype bundles on the Mitchell Spectrograph, which has been taking data for 5 years. We uncovered an interesting behavior when fibers in the corners of the square input array started to show variable and lower throughput on the sky. This was traced to the way the cable was being handled. This cable was 15 m long to allow the Mitchell Spectrograph to be deployed on the HET and each month it was coiled and uncoiled during the mounting process. Twists introduced into the cable resulted in a torsional force at the head, which affected the fibers in the corners, preferentially. This was verified with tests in the lab, which revealed significant stress-induced FRD for these fibers. Shaking out the cable relieved the stress but was only a temporary fix. Interestingly the effect did not show itself until after more than a year of use, so it is possible that the constant handling of the cable caused these fibers to become more sensitive to the torsional stress. In this respect the

long track-record of the Mitchell Spectrograph has proven valuable in evaluating the design. The IFU of the Mitchell Spectrograph has now been replaced with a new shorter model produced by AIP, and the results are very stable.

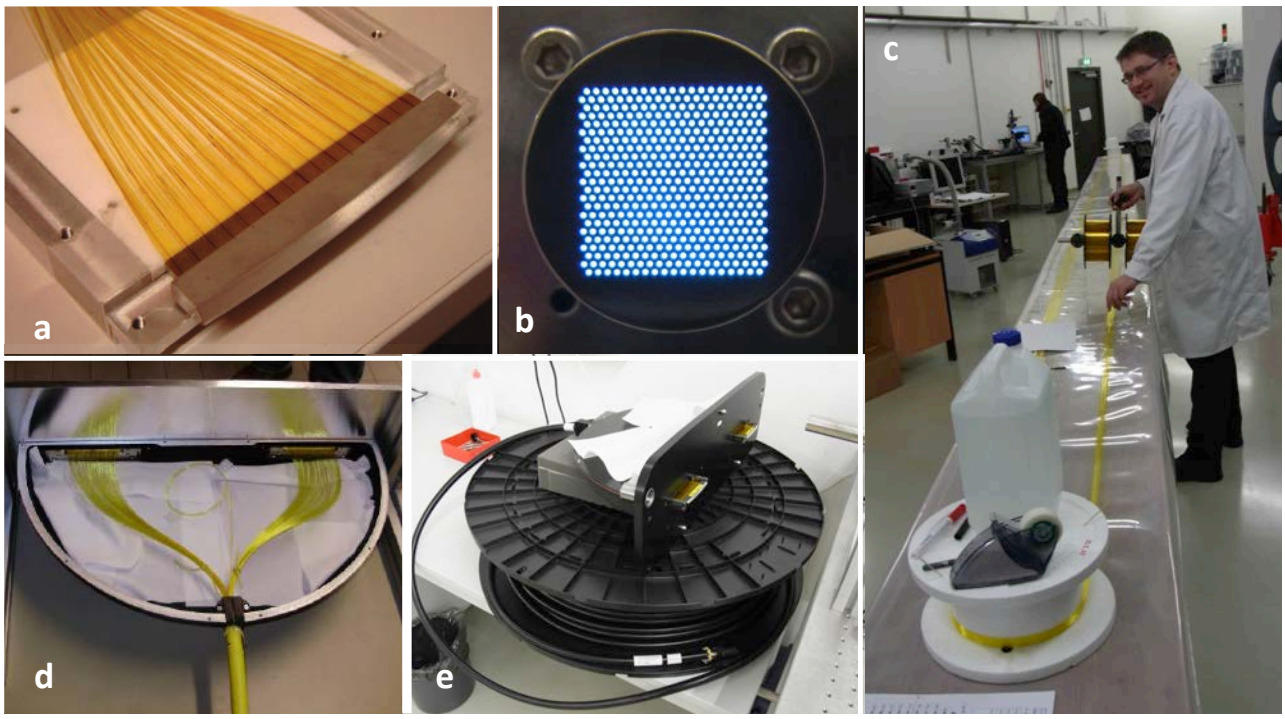

Figure 8. Production of IFU cables at AIP. (a) a slit block with 224 fibers; (b) an input head, back illuminated, with 448 fibers – note the 1/3 fill-factor of the fiber cores; (c) laying out of fiber at AIP; (d) an integrated output slit assembly with two slit blocks mounted and the fan-out of fibers from the conduit; (e) a completed IFU of 22 m length manufactured by Ceram Optec.

The conduit housing the fiber cables underwent an extensive design evaluation and prototyping. It is important that the fiber not piston significantly in and out of the conduit where it exits the cable into the slit box. Such pistoning might occur with changes in axial load or ambient temperature swings, and we were particularly concerned about shipping and handling during installation and avoiding twists. We also wished to minimize the weight of the conduit, which can dominate the total weight, and adopted a custom fully interlocked aluminum conduit with PVC sheathing supplied by Hagitec. The ID is 13 mm. As with our previous cables we have an inner sock of Kevlar to protect the fiber from the internal structure of the conduit. In order to stabilize the length of the conduit we tension this inner sock at assembly so that the conduit is somewhat compressed and the resultant spring constant is high. The Kevlar sock has a minimum diameter chosen so as not to constrict the fiber, but still fit in the ID of the conduit. The Kevlar is tensioned during assembly, which stabilizes the length of the conduit assembly and prevents fibers “pumping” in and out and developing torsional stress. We have taken this design through the full range of motions expected at HET (and more) and not seen any sign of the fiber pistoning in and out of the conduit at its exit.

The exit focal ratio from the cable and the position of the pupil from each fiber at the instrument pupil depend on more than FRD. Tilts of the fibers (individually and as a group) at the input make the exit focal ratio faster, and tilts at the slit cause the pupil to translate in the instrument. The VIRUS optical design allows for 10 mm extra pupil diameter, and all these effects were toleranced and added to the FRD, so that in total at least 95% of the light passes unvignetted through the instrument pupil.

While 7 years of use on the Mitchell Spectrograph has provided information on the durability of IFU cables, we also conducted a more controlled test in order to uncover any design issues related to durability in the production IFUs before committing to full production. In particular, we first wanted to understand how the fibers behave while in motion, and that might depends on the rate of fiber motion. Second, we wished to monitor how the properties of a VIRUS fiber bundle change due to the accumulation of wear. In order to explore these questions we simulated 10.2

years of wear (188.7 km of linear travel) on a single fiber bundle. The simulated motion was carried out between February and May, 2011 on test rig designed and built for this purpose. Results of the lifetime test are described in Ref. 55, and qualified the cable design for final manufacture.

In production, we provide the manufacturers with kits of parts (fiber, mechanical parts, conduit, etc.) and they do the assembly and polishing of the ends. Final integration of the slit blocks into the output slit assembly is done at AIP. We have established three production lines, based on qualification work at several vendors. One is at AIP (Fig. 8), and the others at CeramOptec and FiberWare. Each is capable of producing at least one IFU per month. Acceptance test and evaluation facilities have been set up at AIP. These include microscope examination of polish of the input and output ends against fiducial standards, FRD testing, throughput testing, and fiber mapping and position measurement. A final system test will be performed on each cable with a fiducial spectrograph, generating a report and metadata that will be used by the reduction software and in record keeping. At the time of writing 50 IFUs have been delivered and accepted and are in various stages of final assembly and evaluation.

4.5 Sofware Development

One place where the parallelized nature of VIRUS is a huge advantage is in data reduction software development. Many instruments have suffered from the late arrival of reduction software or from unexpected instrumental features that require the development of new software methods to account for them. Since the VIRUS units will be very close to identical, and very similar to the Mitchell Spectrograph, we have had the advantage of having a full test-bed for the software in operation for several years.

The software for VIRUS must process a highly parallel data stream, quickly, and detect single-line objects, reliably. Development of the final software pipeline for reduction of VIRUS data is being led by MPE. Since VIRUS is naturally a parallel instrument, all the requirements for and attributes of the software have been developed and tested on the prototype. This was a key motivation for the deployment of the Mitchell Spectrograph on the telescope early in the project. Two pipelines have been developed, one in Texas called VACCINE[28] and the other in Munich, called CURE[47]. VACCINE was used primarily to reduce and analyze data from the pilot survey on the McDonald 2.7 m, while the algorithms of CURE are tuned for use on the HET. The difference is driven primarily by the plate scale difference between the telescopes. On the 2.7 m, the fibers are significantly larger than the image size, while on HET they are comparable. This leads to differences in the detection algorithm, but not the data reduction methods. Care is being taken to propagate errors and avoid interpolation through resampling of data, which leads to position-dependent smoothing and can alter the noise characteristics. CURE uses a Bayesian detection algorithm that assigns a likelihood of a source to every (spatial and spectral) resolution element. Tests show robust rejection of cosmic rays and reliable detection of 5-σ line flux objects, as required for HETDEX. The stability requirements for the instrument are driven by the need to know the statistical weight of each pixel, particularly in the spatial dimension, across the fiber profiles, where small movement of the image on the detector can change the weights greatly. We have also demonstrated sky subtraction to the Poisson noise limit, with both pipelines, aided by the fact that most of the fibers of VIRUS are observing sky in any exposure.

We have exploited the advantage to having the ability to exercise software on real data early in the project, and we expect to come on line with a fully operational and debugged pipeline when VIRUS is turned on. This is a key advantage of a highly replicated and hence parallel instrument, particularly since such instruments by definition generate large volumes of data. Software must follow a mass-production model as well.

5. VIRUS PRODUCTION

The development of replicated instruments follows a different path to monolithic designs. Overall, the amount of engineering effort per unit is much lower, but there is a need to undertake more engineering effort to ensure that requirements over an ensemble of instruments are met and to speed the assembly and characterization phases. Following manufacturing best practices, a prototype must be built and preferably used on sky before freezing the design. This step can add significantly to the duration, but forces the confrontation of science requirements with instrument performance and also encourages early development of the data reduction pipeline. These factors reduce overall risk. Following any changes from the prototype, parts are ordered and the production line is set up. Before full-scale production begins, the "First Article" unit is constructed and evaluated. Ideally, the First Article is followed by a limited production run, but

the volume of ~100 units that we are dealing with in VIRUS does not necessitate this step. We produced a first article and then 3 units in the first production run and use them for lab testing at each institution.

In the process of developing VIRUS, we followed this protocol and learned a lot from the prototype (Mitchell Spectrograph, aka VIRUS-P[4]), which we used to undertake the HPS, ensuring the science requirements were met and software pipelines developed[28]. In taking the prototype to a replicable design, we adopted several principles and discovered rules of thumb as follows:

- Finding the lowest cost per pixel for the detector is a key driver. For VIRUS this led to the format of ~2kx2k pixels, which at the time offered very high yields and reduced risk for the manufacturer sufficiently that they were prepared to accept small margins. We purchased 200 detectors, from several wafer runs. At the present time, the balance may be starting to shift towards 4kx4k detectors, but 2kx2k format remains the lowest cost per pixel.
- Use of liquid nitrogen (LN) to cool CCD detectors to ~-100 Celsius working temperature. Early on, we undertook a trade-off cost and reliability for the VIRUS cryogenic system, which strongly favoured a distributed LN system over a large number of closed-cycle cryocoolers. Thermo-electric cooling is inadequate for the low-noise application of spectroscopy. VIRUS uses a novel heat exchanger to cool the detectors without having LN inside the cryostats, facilitating removal of the cameras for maintenance[43,44]. MUSE also adopted LN as the coolant, with a direct flow system[45].
- Following trade-off, we settled on f/1.3 as the on-axis focal ratio for the fastest camera that can be made and aligned in quantity. This focal ratio is well matched to the plate scale of 10 m class telescopes and the 15 μm pixel size of modern CCD detectors. For VIRUS we had to choose a catadioptric Schmidt-based design for both collimator and camera with a total of 6 components (including two aspheric refractive elements) due to the need for UV coverage[35]. The cost and throughput is very competitive with refractive designs, but necessitated a larger pupil size due to the obstruction of the detector head.
- For the optic sizes of around 200 mm used in VIRUS, the cost per component asymptotes around quantity a hundred. This is because at that point the majority of the cost is in the material, rather than the figuring.
- Volume phase holographic gratings (VPHGs) are cost-effective in quantity and offer the ability to tune the design. In large quantities, this is also true of surface-relief gratings, where a new master can be ruled, but VPHGs offer greater durability, higher efficiency, and lower scattering, particularly if the design is used in transmission, which aids certain mechanical aspects of the design. We supplied the VPHG manufacturer with a custom tester to address specifically our requirements on first order diffraction efficiency and scattered light, and over the course of production this was used to hone the production methods to improve performance[41].
- Careful design of mechanical components is needed to facilitate mass production, and the production method needs to be factored into the design. This is particularly true for small parts that were replicated in quantities up to 800 with computer numerically controlled (CNC) and electro-discharge machining (EDM) techniques[32-34,49]. Use of modern metrology equipment such as coordinate measuring machines (CMM) should be factored into the design for quality control and alignment.
- Use of Aluminium for all structure components, except those requiring high stability to temperature changes (e.g. focus references) for which Invar 36 was used. Flexures ensure controlled compliance between dissimilar materials. This design principle ensures alignment stability over a wide range of ambient temperature. While VIRUS is mounted in large clean-room enclosures, it sees the full range of ambient temperature change since the enclosures must not interfere with the dome-seeing environment.
- Use of castings and large monolithic parts fabricated with CNC mills. Larger mechanical components should be fit to the capacity of CNC mills and, concentrating precision in a few features is another way to reduce overall cost[49]. On VIRUS we used aluminium and Invar 36 castings with a small amount of post machining, and even utilized cast-aluminium for the camera cryostats[49,32]. The time-cost of setting up castings for post-machining should be weighed against the material cost of machining a part directly out of metal stock. The outcome of the trade depends on the relative costs of machine time and labour, since it is now becoming common practice to leave machines running overnight with limited supervision.
- Simplifying assembly as far as possible and concentrating the alignment problem into a small number of components reduces the effort needed to take the spectrographs from parts to the telescope. Designing dedicated alignment tools and addressing bottle-necks by having parallel lines reduces production time, but these steps are labour intensive, still. We have found the final alignment to be a limiting step with the limited effort available. A very deterministic alignment procedure based on wavefront analysis does make it possible for less technically skilled personnel to undertake the task[56-58].

- VIRUS is not general purpose, so we could focus the design and choice of components in an optimized manner. Even so, the design can be adapted to a wide wavelength range as is evidenced by the new HET LRS2 low resolution spectrograph that covers 370-1050 nm by slicing the wavelength range between four VIRUS unit channels[59].

At the time of writing we are 1/2 the way through production of VIRUS and plan to begin deployment in late 2014. Table 1 presents the current and projected production of VIRUS units. In total, the 75 units will contain ~15,000 parts (not including fasteners) and 700 km of fibre. The goal is to reach 78 deployed units by mid 2015 and to start the HETDEX survey in Fall 2015. All told about ½ the total cost has been expended on the spectrographs and IFUs, ¼ on the detector system, and ¼ on engineering labour and data reduction software development.

	Cumulative Totals for VIRUS Production by Quarter									
	2013 Q1	2013 Q2	2013 Q3	2013 Q4	2014 Q1	2014 Q2	2014 Q3	2014 Q4	2015 Q1	2015 Q2
IFUs manufactured & accepted	10	20	26	36	45	52	62	67	73	78
IFUs integrated			14	23	30	30	42	65	71	78
IFUs tested and shipped								32	70	78
Cameras assembled	3	12	25	29	29	40	64	78	78	78
Collimators assembled	12	36	60	65	65	65	75	78	78	78
Spectrographs aligned			8	17	27	39	63	78	78	78
Spectrographs characterized						8	44	78	78	78
Spectrographs shipped to HET								38	78	78

Table 1. Current and projected production figures for VIRUS units and IFUs. The requirement is to deploy 75 units and the goal is 78 units, the maximum that can be accommodated in the VIRUS enclosures

6. VIRUS ALIGNMENT AND CHARACTERIZATION

Following assembly of collimator units at TAMU and cameras at UT Austin, the spectrographs are integrated at UT Austin and aligned. The alignment procedure involves attaching an adjustment back to the camera cryostat, in pace of the regular back, that incorporates ferrofuidic vacuum feed-throughs for adjustment and locking of the camera mirrors (Fig 9(b)). We also allow small adjustments of the collimator position, which comes pre-aligned from TAMU at the 0.1 mm level. Experience with aligning VIRUS-P highlighted the likely bottle-neck of this step in the large-scale production and led us to develop a deterministic alignment procedure that utilizes moment-based wavefront sensing (MWFS) analysis[56-58]. This moment-based wavefront sensing (MWFS) method relies on the geometric relation between the image shape moments and the geometric wavefront modal coefficients. The MWFS method allows a non-iterative determination of the modal coefficients from focus-modulated images at arbitrary spatial resolutions. The determination of image moments is a direct extension of routine centroid and image size calculation, making its implementation easy in the alignment of real systems like VIRUS.

The alignment procedure is as follows: using Hg+Cd lamps as the line source, we move the collimator mirror along the optical axis by adjusting three manual micrometers on the back of the mirror taking exposures at five modulations (positions) per run. The IFU input is masked so that the images of the fibers do not overlap on the detector. The acquired images are then processed through the MWFS pipeline software, where the modal coefficients associated with individual fiber images and their errors are estimated. Each estimated coefficient is then fitted by a quadratic curve across the slit or the wavelength dimension, resulting in the gradients of the coefficient in both directions across the CCD. The gradients are then used to determine the required tip and tilt angles of the camera mirror and/or the collimator mirror. The software predicts the required move for both optics to achieve alignment. We restrict the motion of the collimator since the optics come pre-aligned to a certain level from TAMU and there is some degeneracy between camera and collimator moves. For the defocus term, the zero-th order curve fit value provides the overall piston focus correction. We use the piston focus estimate only as a guidance and do not attempt to completely zero out the focus term because the zero defocus in fact results in slightly larger PSF. Therefore, the final focus adjustment is done by a combination of the visual inspection of the fiber images and then confirmed by the final contrast test.

Throughout the alignment of the VIRUS units so far (30 units), we typically needed two modulation runs and thus two rounds of corrections. After these corrections, we fine-tune the focus by the contrast test on the fully exposed IFU images without the IFU mask. In the contrast test, we slice through the centers of the fully exposed fiber images in the slit dimension and then compute the peak value of each fiber image and the valley value of between two fibers. The requirement that the valley be lower than 50 percent of the peak is the root requirement of the error budget for the

optical fabrication and alignment. We compute the standard contrast of (Ipeak −Ivalley)/(Ipeak +Ivalley) for each fiber image. The requirement is that 90 percent of the fiber images across the CCD must have the contrast value higher than 60 percent (equivalent to a cross over point of 25% of the peak). This requirement is much tighter than the original 50% cross-over point requirement that we established in tolerancing the optical design for production, reflecting the power of this method to greatly exceed our requirements by making the alignment error contribution to the image sizes quite negligible. The image quality performance of every VIRUS production unit has exceeded that of VIRUS-P by a substantial margin. The contrast test gives a quite sensitive feedback on the focus adjustment.

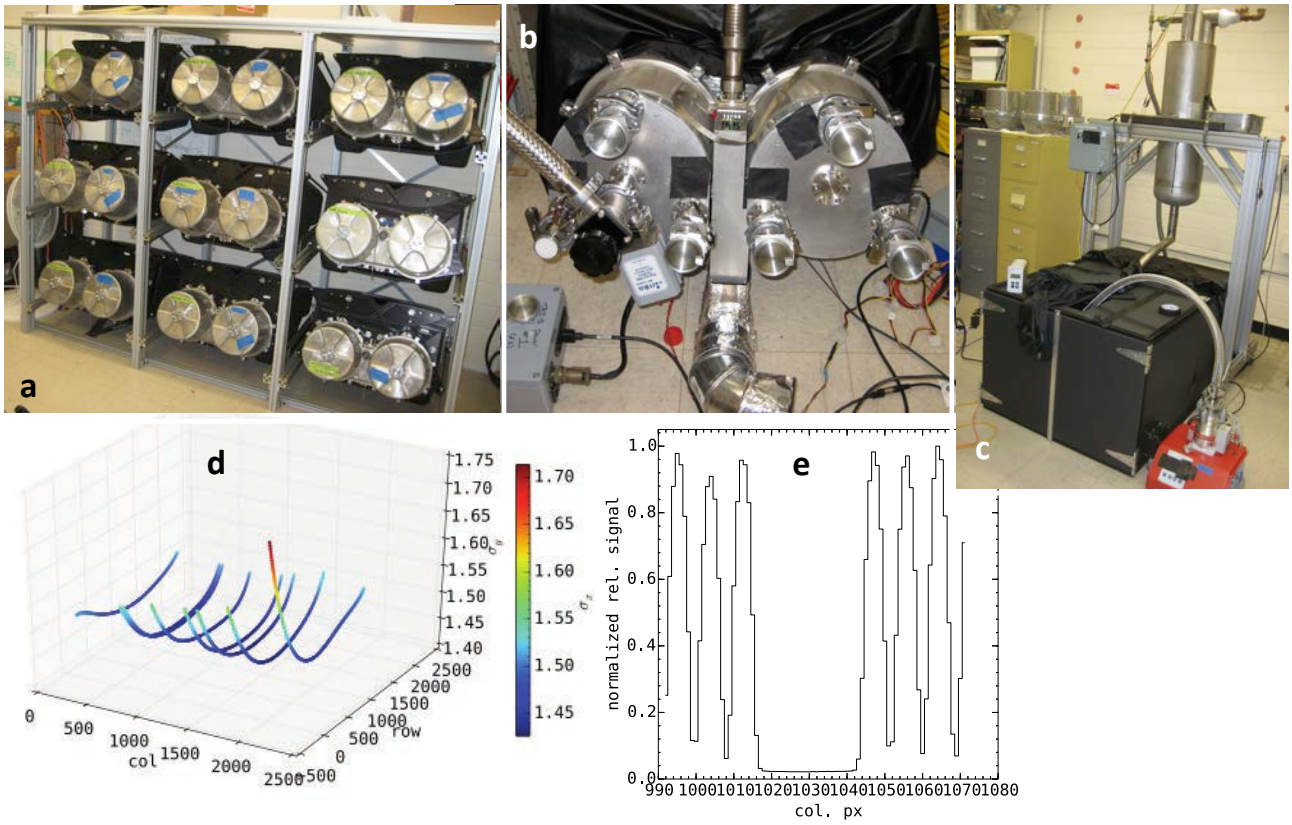

Figure 9. Images of production and alignment of VIRUS spectrograph units. (a) shows one of several racks with aligned units awaiting final characterization; (b) shows a unit undergoing alignment with the adjuster back installed on the camera cryostat; (c) characterization enclosure in a separate lab at UT Austin; (d) example output from LabCure showing the image quality in the cross-dispersion direction (expressed as in the σ of a Gaussian fit, in pixels); (e) another example output showing a cross cut of flat-field spectra near the center of the detector; note the very good separation of the individual spectra and the low level of scattered light between the banks of fibers.

While the analysis underlying the MWFS technique is fairly complex, we have scripted the alignment scheme and have been able to train non-expert users to achieve results that are exact and deterministic. This situation contrasts with the very inexact process usually employed to measure image size over the detector and make incremental adjustments to minimize it, as was employed on VIRUS-P. The time required for the alignment is roughly half a day per channel plus time to pump the cryostat and cool the detectors. We have achieved a steady state of 2 units (4 channels) per week, approximately twice that required to complete the process by the end of 2014.

Following alignment, VIRUS units undergo a characterization before being packed for storage and eventual transport to the HET. Figure 9(c) shows the characterization station at UT Austin, which is located in a separate lab that can be darkened sufficiently to ensure no stray light for the tests. Previously we had this set up in the alignment lab and that led to inefficiencies for both activities. Deuterium lamps are used for flat-fielding and Hg+Cd line lamps for wavelength determination. In addition, a unit that mounts in place of the IFU head and provides a continuous illumination of the two slits rather than the highly modulated IFU output is utilized to provide the source for pixel-flat-

fields of the detector, free of the spatial dimension fiber modulation. This is important for generating maps of the pixel to pixel QE variations and to identify bad pixels. Photon transfer curves are generated to confirm read noise and gain of each channel, and sets of bias and dark frames are recorded to act as a reference once the units are installed at HET. Scripts are being developed to obtain characterization datasets in conjunction with the VDAS control system and a lab version of the Cure data reduction package (LabCure) has been developed to provide a digest of the results for reports on each unit. The metadata generated by the characterization step travels with the units to the mountain and will be part of the data delivery when in use. Figure 9(d,e) shows examples of the output from LabCure, and highlights the exceptional image quality being obtained by the alignment protocol.

7. VIRUS INFRARSUCTURE ON HET

The VIRUS spectrograph units take up a large volume and require a distributed liquid nitrogen (LN) cooling system[43,44]. The infrastructure to support VIRUS is a significant undertaking and is being integrated with the deployment of the WFU. Since the wavelength coverage of VIRUS extends down to 350 nm, the average fiber length had to be minimized commensurate with keeping the mass of the instrument off the telescope structure and providing sufficient access to the primary mirror and tracker with the HET man-lifts and crane. Following extensive optimization and evaluation by HET staff, we settled on a configuration with VIRUS units housed in two large enclosures flanking the telescope structure and riding on a separate air-bearing system during rotation of the telescope in azimuth (Fig. 1).

VIRUS units and the new LRS2 low-resolution spectrograph are housed in the large enclosures mounted on each side of the telescope (Fig. 10(a)). They are supported by the VIRUS support structure (VSS[7]) framework designed to carry the weight of the enclosures and spectrographs without connecting to the main structure of the telescope in order to ensure no coupling of wind-shake-induced motion into the tracking of the telescope. The VSS is shown in Figure 10 both in rendering and as installed on the telescope. For changes in azimuth, the VSS rides on its own set of air bearings and is dragged by the main structure drives through loose linkages. When the structure is placed down, there is no significant coupling between the structures except through the concrete ring-wall pier at the base. The VSS was designed to withstand a catastrophic deceleration from full rotation speed without collapsing, though damage to the pier would be inevitable. We have not encountered any such incident in operating HET for 13 years.

The two large VIRUS enclosures are mounted to the VSS and are essentially sealed clean-rooms with a heat removal system to avoid degradation of the seeing by the heat generated by the detector controllers and electronics from escaping to the dome by convection or air leaks. They are based on large steel space-frames manufactured by SMK Manufacturing with skins and removable hatches to provide access to both sides of the spectrograph for camera maintenance and IFU access, respectively. The steel frames (Fig.10(c)) were analyzed with FEA to withstand the same impulses as the VSS. They have been procured by MDO and are being outfitted with hatches, seals, cables and the heat removal system by TAMU[60]. Tests of lightweight simple hatches that can be produced in quantity have shown excellent performance for air leakage rate.

The heat removal system is separate for each enclosure. They use ambient temperature facility glycol as the primary coolant fluid with a 600 W “Thermocube” thermoelectric cooler on each side providing the ability to tune the temperature of the circulating air to keep the overall environment close to ambient temperature. Heat removal is needed to keep the VIRUS detector controllers from overheating and to remove the heat they generate so it does not enter the dome and degrade the seeing environment. Tests of prototype PVC ducting and custom attachment boot to the VIRUS controllers show excellent performance[60]. Air is drawn through the controllers by the system and cold HEPA-filtered air is returned at the top of each sealed enclosure[60]. The enclosures will be delivered to HET between Sept and October so they are ready for VCS installation in November[7].

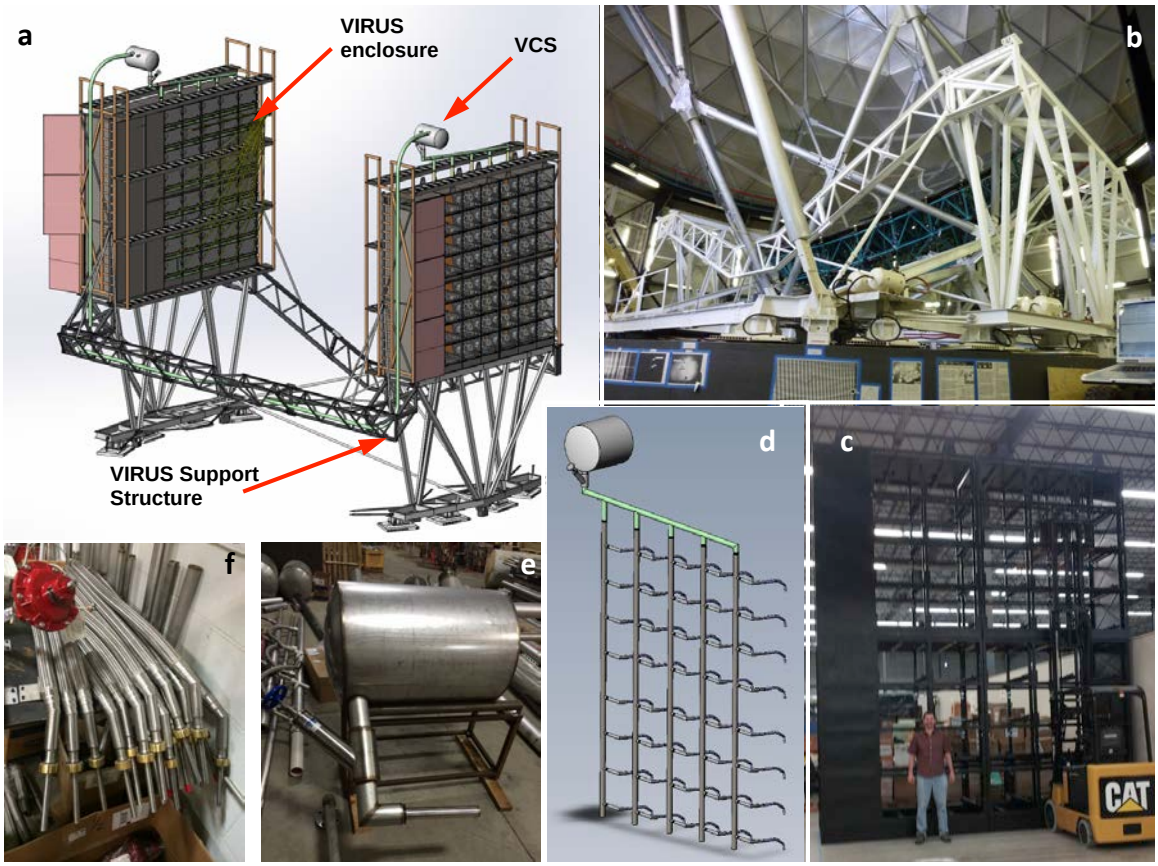

Figure 10: VIRUS infrastructure in development. From top left, clockwise (a) rendering of the VIRUS support structure (VSS), enclosures, and VIRUS cryogenic system (VCS), note the four air bearings at the base of each side, on which the structure lifts when the telescope changes azimuth; (b) the VSS installed, sitting on HET ringwall; (c) enclosure weldment for one side assembled at TAMU with a Québécois for scale; (d) schematic of the VCS for one enclosure, showing vertical sections each feeding 8 cameras and the phase separator tank; (e) and (f) show a phase separator and flex lines with bayonets that connect to individual VIRUS cameras at Midwest Cryogenics.

The distributed and large-scale layout of the VIRUS array presents a significant challenge for the cryogenic design. Allowing 5 W heat load for each detector, with all losses accounted for and a 50% margin, the cooling source is required to deliver 3,600W of cooling power. We engaged George Mulholand of Applied Cryogenics Technology to evaluate the options and provide an initial design[43]. Following a trade-off between cryocoolers, small pulse-tubes and liquid nitrogen based systems, it is clear that from a reliability and cost point of view liquid nitrogen is the best choice. The problem of distributing the coolant to the distributed suite of spectrographs is overcome with a gravity siphon system fed by a large external dewar. A trade-off between in-situ generation of the LN in an on-site liquefaction plant, and delivery by tanker has been made, with the result that the delivery option is both cheaper and more reliable[43].

An important aspect of the cryogenic design is the requirement to be able to remove a camera cryostat from the system for service, without impacting the other units. This is particularly difficult in a liquid distribution system. A design has been developed that combines a standard flexible stainless steel vacuum jacketed line (SuperFlex) to a cryogenic bayonet incorporating copper thermal connector contacts into each side of the bayonet[43,44]. When the bayonet halves are brought together they close the thermal contact. The resulting system is completely closed, i.e., it is externally dry with no liquid nitrogen exposure. The camera end of the connector is connected by a copper cold finger to the detector. This design has another desirable feature: in normal operation the SuperFlex tube slopes downwards and the bayonet is oriented vertically. Liquid evaporation will flow monotonically up in order to avoid a vapor lock. If the bayonet is unscrewed and raised upwards, a vapor lock will occur and the bayonet will be cut off from the cooling capacity of the liquid nitrogen. This effectively acts as a “gravity switch”, which passively turns off cooling to that camera position.

We have made extensive tests on prototypes, applying heat loads to the bayonet, which have performed very well[44]. The temperature rise across the connection is $\Delta T \sim 1.8$ K/Watt of load at 80 K. Modeling of the full thermal path has been undertaken, under the requirement of having the CCD temperature at -140 C, with no heater power. The performance of the bayonet is significantly better than the requirement, and represents less than 20 K temperature rise across the connection for the expected load. We run the CCDs at about -110 C, controlled via heating resistors and a control loop based on an RTD sensor. The performance of the bayonet is not changed when the connection is broken and remade.

We have been running a lab cryogenic system for VIRUS testing for the past 4 years[32]. It is a microcosm of the final VCS having a large external dewar, a header tank with "keep full" auto-fill system, and a single flex line and bayonet. The system is extremely reliable, and has been used to demonstrate that the VIRUS cryostats will hold vacuum, when kept cold, for at least 4 months without external intervention such as use of an ion pump. This performance allows us to avoid the cost of adding ion pumps and vacuum gauges to each camera, and instead rely on a maintenance regimen at HET that regularly warms, vacuum pumps, and then re-cools the cryostats in-situ, every 3-4 months. Based on the extensive prototype testing we are confident that the full cryogenic system will be robust. We have been using such systems in labs at VIRUS partner institutions for several years, and find them very easy to use.

The contract for the fabrication of the VCS is awarded to Midwest Cryogenics. In the process of working with Midwest Cryogenics we discovered issues associated with the manufacturability and maintainability of our initial design[35,36] for the VCS components that reside in/on the VIRUS spectrograph enclosures. After working closely with Midwest Cryogenics a much-improved design emerged (Fig. 10(d)). The design is easier to fabricate and maintain, has lower heat loss, and is significantly less expensive. However, because the new design is somewhat different than the initial design (that was recommended by our very seasoned cryogenic system expert George Mulholand) we felt it necessary to qualify the design by conducting a functional performance test.

Before proceeding with fabrication, a full-scale prototype of one of the vertical distribution pipes was fabricated and functionally tested at Midwest Cryogenics. The goal of the test was to verify that the pipe sizes would not compromise the two-phase flow thereby reducing the system's ability to remove heat from the camera cryostats. Utilization of test bayonets in place of actual VIRUS camera cryostats greatly simplified the test logistics and reduced test cost. Each bayonet was equipped with an RTD (0.1°C resolution and ±0.2°C accuracy) and a 20W heater. At the beginning of each test the bayonets were cooled with LN. After they reached thermal equilibrium their temperature was monitored as various combinations of the bayonet heaters were turned on to simulate anticipated and extreme heat loads. Test bayonets were calibrated in our lab against an actual VIRUS camera cryostat prior to conducting tests at Midwest Cryogenics.

Test results indicated that the new VCS design meets our functional performance requirement. When we tried heating in extremis several bayonets to try and disrupt the cooling system we found the heating to not be disruptive, which is encouraging for the functioning of the fully populated vertical. We tried both heating seven as well as heating one at a time (for each bayonet) and found no problems. Note that the test bayonet heaters were set to 20W for these tests, so they were producing 2.3 times more heat than a VIRUS cryostat. The measured fluctuations of the unheated bayonet (when the other seven were set to 20W) was no more than about ±0.5°C; well within the requirement of ±1.5°C.

At the time of writing, the first phase of VCS installation is complete, running from the location of the external tank, through the azimuth wrap of the HET and many parts are fabricated (Fig 10(d,e)). The second phase will be executed after the enclosures are in place, since the VJ piping needs to be threaded into the enclosures. It will then be commissioned prior to installing spectrographs. The VCS is due to be installed by the end of November 2014. The 11,000 gallon vacuum jacketed holding dewar will be installed by Praxair in October 2014. It will have in excess of 4 weeks operation capacity and a 6,000 gallon delivery of LN will be required every two to three weeks. More details of the tests and safety system are given in Ref. 7.

8. THE VIRUS FUTURE

VIRUS was designed from the outset to allow exchange of gratings to change wavelength ranges and resolutions, and the Mitchell Spectrograph is used on the McDonald 2.7 m Smith Telescope with four different VPH gratings. Due to the large size of the fibers projected on the sky, it is very sensitive for low surface brightness extended features, for which the sensitivity surpasses that of instruments on the largest telescopes. In addition to this flexibility and sensitivity, the

generic nature and massively replicable characteristic of the instrument can allow us to adapt the instrument to a wide range of not only telescope diameters (1m ~ 40m), but also observing modes (single to multiple objects), in a very cost-effective manner. On small telescopes, the IFU can cover very large fields of view with large spatial elements ideal for studying resolved galaxies, while on large telescopes the same IFU can observe single objects in varying image quality, while obtaining a simultaneous background observation. VIRUS allows many different slicing modes between field and wavelength coverage/resolution, and a few of them are illustrated in the following examples.

The previous HET Low-Resolution Spectrograph[61] was incompatible with the WFU and will be replaced with a more capable broad-band fiber-fed instrument based on VIRUS, called LRS2[59]. It takes advantage of the fact that VIRUS was designed to be easily adapted to a wide range of spectral resolutions, and wavelength ranges by changing dispersers and optics coatings. LRS2 is fed by a 7x10 arcsec^2 lenslet coupled fiber IFU, covers 350-1100 nm, simultaneously at a fixed resolving power R~1800, with the wavelength range split with dichroics into four channels shared between two VIRUS units, one for the blue and red wavelength range (370 - 630 nm) and the other for the red and far-red range (630-1050 nm). It uses the multiplex power of VIRUS to cover wavelength, rather than wide area. Only minimal modification from the base VIRUS design in gratings (grisms for both units) and in the detectors (to thicker CCDs for the far-red unit only) is required. We expect to deploy LRS2 when we install VIRUS. LRS2 is a powerful instrument serving the HET strengths in survey follow-up, synoptic observations, and transient events. It will be particularly useful for following up emission-line objects detected with VIRUS at higher resolution, and can be used in parallel with VIRUS.

A highly-replicated spectrograph has not been proposed as a first-light instrument for any of the ELTs. The huge grasp of MUSE[9] and VIRUS makes them quite adaptable to ELTs and certainly the scale of these instruments is "extremely large" (MUSE takes up a whole Nasmyth platform at VLT and VIRUS fills two clean-room enclosures, each 6x6x1.5 m^3). The power of replication is illustrated in Figure 11, following Bershady[62,63] and adapted from Ref. 10, we plot instrument areal grasp (AΩ) versus spectral power (the product of the number of spectral resolution elements and the resolving power $N_\lambda R$, where $R=\lambda/\delta\lambda$ for wavelength λ and spectral resolution $\delta\lambda$) as a useful metric in following the evolution of total instrument grasp (the product of the two quantities)[10]. In Figure 11 we show the locus of these quantities for different-sized detectors, extending up to the maximum current CCD pixel-count (N_{pxl}) used in spectrographs of about 8kx8k pixels (or 6kx12k) achieved on single wafers or small mosaics. The loci for each detector size are plotted for the following instrument parameters: f/1.3 camera focal ratio (a practical limit for refractive optics), 15 μm pixel size typical of modern CCDs used in astronomy, 4.0 pixels per resolution element with a packing efficiency of 65% to allow for separation of spectra on the detector, and resolving power of R=1000 typical of large survey spectrographs on a range of telescope sizes. Fig. 11(left) shows the metric for IF spectrographs, multi-object spectrographs (MOS) and replicated instruments. Replicated instruments are defined as any with more than one copy, but the highly replicated instruments are emphasized with larger symbols. The loci at constant N_{pxl} are diagonal and form parallel lines with increasing N_{pxl}. The loci reflect the fact that the available detector area is divided between spatial and spectral elements depending on details of instrument design driven by science requirements. Available detector size is a primary driver of the evolution of spectrograph capability. The shaded region of beyond the 8kx8k N_{pxl} locus in Figure 11 is the domain of replicated instruments[10].

Three ELTs are under development. All have a significant science emphasis on spatial resolution supported by adaptive optics (AO), but each has a wide field survey spectrograph designed to work with natural seeing or Ground Layer AO. In Figure 11(right) we present the grasp and spectral power of proposed ELT instruments DIORAMAS (EELT[64]), MOBIE (TMT[65]), and GMACS (GMT[66]), compared to VIRUS and MUSE and other replicated instruments on VLTs. DIORAMAS has 4 replicated channels and GMACS is plotted for a four-spectrograph instrument that strains budgets. The locations of the ELT instruments indicate why high grasp through replication will become essential to exploit the vast amount of information being gathered, not just for large surveys as is the focus on smaller telescopes.

As an example of how large-scale replication can address some of the challenges of instrumenting the next generation of telescopes, we consider how VIRUS might be adapted to the 25 m Giant Magellan Telescope. As mentioned above, the relatively poor image quality of HET, coupled with its 10 m pupil size, qualify HET as the world's smallest ELT, since the instrumentation challenges are very similar. This is trivially illustrated by the fact that the VIRUS fibers project to 1.5 arcseconds at HET and would subtend 0.6 arcseconds on GMT, well matched to the excellent site seeing at the Las Campanas site. In principle, VIRUS could observe 16,000 objects in traditional single-fibre MOS mode, with a sky fibre assigned to each object, to ensure adequate sky-subtraction on faint targets, though the fibre positioning system would be frightening.

More interesting would be to couple VIRUS with an adaptive focal surface system such as the proposed GMT Many Instrument Fiber System (MANIFEST[67]) and use the grasp of VIRUS to feed dIFUs of a range of sizes. VIRUS units could also be configured with different wavelength ranges and resolutions depending on the application, and no doubt the balance of detector area would be shifted towards wavelength coverage and resolving power. This configuration is very similar to that proposed for GMACS in combination with MANIFEST. The 4-unit GMACS would accommodate 420 dIFUs, and cover a wide spectral range at higher resolution than the lower resolution imaging spectrograph mode. The 0.25 arcsecond diameter spatial element of the dIFU is much better matched to the camera focal ratio and pixel size of GMACS, which is why the GMACS/MANIFEST point stands out as having the greatest total instrument grasp in Figure 11. This point illustrates the power of image slicing for ELT applications, since the slicing allows much better use to be made of the total pixel count in the large CCD arrays proposed for GMACS.

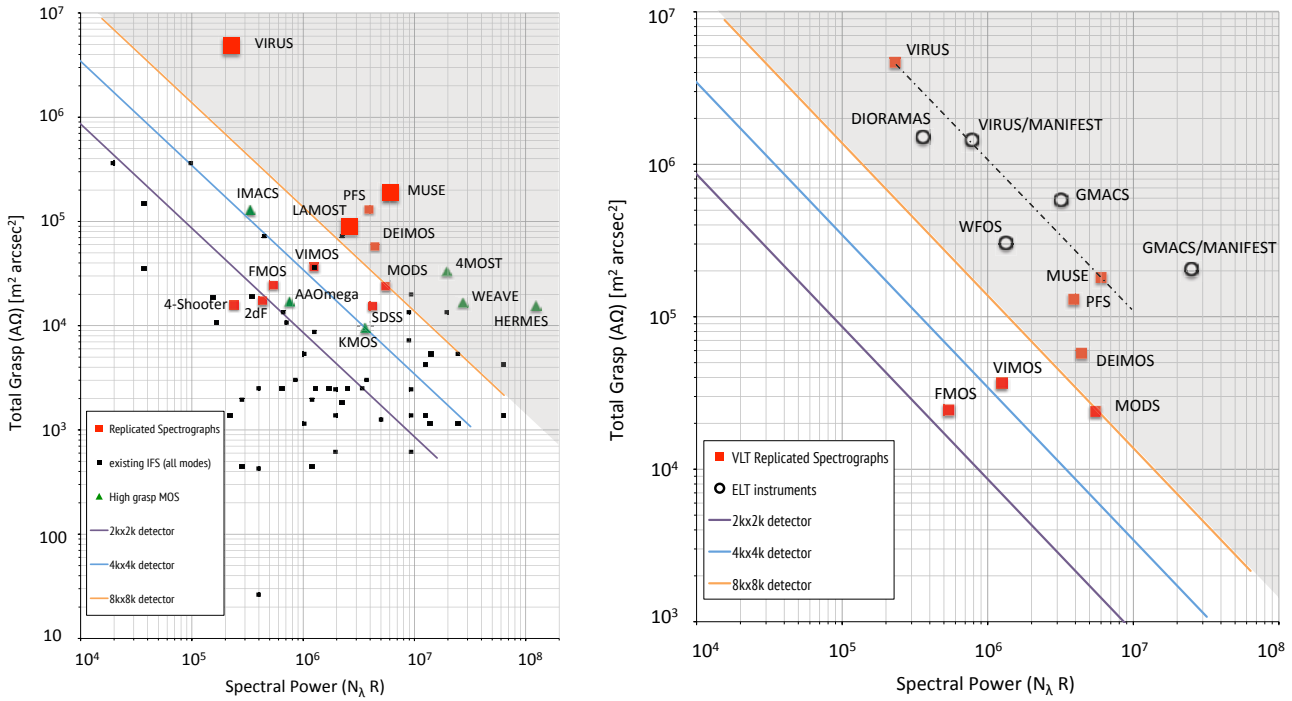

Figure 11. Performance metrics for VIRUS compared with other instruments, both existing and planned. Total Grasp is the product of telescope collecting area and area subtended by the sky spatial elements. Spectral Power is the product of the resolving power and the number of spectral resolution elements. Diagonal lines represent the loci of instruments with varying total detector pixel count. See Ref. 10 for further details. Left, integral field spectrographs (IFS), high multiplex multi-object spectrographs (MOS) and replicated spectrographs compared. The highly replicated instruments are emphasized by larger symbols. The grey shaded region is the zone of replicated instruments. Right, existing replicated instruments compared to proposed survey instruments on ELTs. See text for details.

As a specific example of what VIRUS could do in this context, it would be possible to deploy 2000 19-element dIFUs with 1.7 arcsec field, sampled at 0.33 arcseconds, accommodated by VIRUS with 150 μm diameter fibers. These dIFUs are very similar to those considered for the GMACS/MANIFEST combination. The MANIFEST positioning system could deploy these 2000 dIFUs anywhere in the 20 arcminute field of GMT and the wavelength ranges of the VIRUS units could be selected by object. The resulting VIRUS point is plotted on Figure 11(right) as VIRUS/MANIFEST. Note that this highly competitive replicated spectrograph is identical to VIRUS except for an exchange of dispersers and only uses 2kx2k CCDs. It has not been optimized for the GMT, other than to consider the configuration of the IFUs. Based on experience with VIRUS, it could be realized for ~$20M, a fraction of the projected cost for GMACS or the other ELT instruments.

This toy example simply illustrates the power that replication can bring to bear on the challenges posed by the 50 million spatial resolution elements available in the GMT or other ELT field of view, even without any AO. Of order a percent of the spatial elements will have an object, many of which will be of interest, so taking full advantage of these

telescopes will be a significant challenge that replication can begin to address. Thousands of targets will be available, rather than hundreds. The ability to feed multiple instruments, whether VIRUS-like or not, through an adaptable targeting system like MANIFEST will also be an important part of any solution.

9. SUMMARY AND STATUS

HETDEX, consists of the HET WFU, VIRUS, and the blind spectroscopic survey of 420 sq. degrees. Completion of the WFU and commissioning of VIRUS is projected for mid 2015. VIRUS infrastructure at HET, consisting of thermally-controlled enclosures and large distributed liquid nitrogen cooling system, will be installed this calendar year. When complete, the combination of the 10 m wide-field HET with the grasp of VIRUS, with more then 33,000 fibers on sky, will create a unique facility that will be able to survey vast areas of sky spectroscopically for the first time.

ACKNOWLEDGEMENTS

HETDEX is run by the University of Texas at Austin McDonald Observatory and Department of Astronomy with participation from the Ludwig-Maximilians-Universität München, Max-Planck-Institut für Extraterrestriche-Physik (MPE), Leibniz-Institut für Astrophysik Potsdam (AIP), Texas A&M University, Pennsylvania State University, Institut für Astrophysik Göttingen, University of Oxford and Max-Planck-Institut für Astrophysik (MPA). In addition to Institutional support, HETDEX is funded by the National Science Foundation (grant AST-0926815), the State of Texas, the US Air Force (AFRL FA9451-04-2-0355), by the Texas Norman Hackerman Advanced Research Program under grants 003658-0005-2006 and 003658-0295-2007, and by generous support from private individuals and foundations.

Financial support for innoFSPEC Potsdam of the German BMBF program *Unternehmen Region* (grant no. 03Z2AN11), and of Land Brandenburg, MWFK, is gratefully acknowledged. MMR also acknowledges support by the German BMI program *Wirtschaft trifft Wissenschaft*, grant no. 03WWBB105.

We thank the staffs of McDonald Observatory, HET, AIP, MPE, TAMU, IAG, Oxford University Department of Physics, the University of Texas Center for Electromechanics, and the University of Arizona College of Optical Sciences for their contributions to the development of the WFU and VIRUS. Matthew Bershady kindly supplied his compilation of IFS characteristics used in Figure 11. We thank Chris Clemens and Jim Arns for helpful discussions during the development of the gratings for VIRUS.

REFERENCES

[1] e.g. Ciardullo, R., Gronwall, C., Wolf, C., et al., "The Evolution of Lyα-emitting Galaxies between z = 2.1 and z = 3.1", ApJ 744, 110 (2012)

[2] e.g. Rauch, M., et al., "A Population of Faint Extended Line Emitters and the Host Galaxies of Optically Thick QSO Absorption Systems," ApJ, 681, 586, (2008)

[3] Hill, G.J., MacQueen, P.J., Palunas, P., Kelz, A., Roth, M.M., Gebhardt, K., and Grupp, F., "VIRUS: a hugely replicated integral field spectrograph for HETDEX", New Astronomy Reviews, 50, 378 (2006)

[4] Hill, G.J., MacQueen, P.J., Smith, M.P., Tufts, J.R., Roth, M.M., Kelz, A., Adams, J.J., Drory, N., Barnes, S.I., Blanc, G.A., Murphy, J.D., Gebhardt, K., Altmann, W., Wesley, G.L., Segura, P.R., Good, J.M., Booth, J.A., Bauer, S.-M., Goertz, J.A., Edmonston, R.D., and Wilkinson, C.P., "Design, construction, and performance of VIRUS-P: the prototype of a highly replicated integral-field spectrograph for HET", Proc. SPIE, 7014-257 (2008)

[5] Hill, G.J., Cornell, M.E., DePoy, D.L., Drory, N., Fabricius, M.H., Kelz, A., Lee, H., Marshall, J.L., Murphy, J.D., Prochaska, T., Tuttle, S.E., Vattiat, B.L., Allen, R.D., Blanc, G., Chonis, T.S., Gebhardt, K., Good, J.M., Haynes, D.M., MacQueen, P.J., Rafal, M.D., Roth, M.M., Savage, R.D., and Snigula, J.M., "VIRUS: production of a massively replicated fiber integral field spectrograph for the upgraded Hobby-Eberly Telescope," Proc. SPIE, 8446-21 (2012)

[6] Hill, G.J., *et al*., "Current status of the Hobby-Eberly Telescope wide field upgrade," *Proc. SPIE*, 8444-19 (2012)

[7] Hill, G.J., Drory, N., Good, J., Lee, H., Vattiat, B.L., Kriel, H., Bryant, R., Elliot, L., Landiau, M., Leck, R., Perry, D., Ramsey, J., Savage, R., Damm, G., Fowler, J., Gebhardt, K., MacQueen, P.J., Martin, J., Ramsey, L.W., Shetrone, M., Schroeder, E., Cornell, M.E., Booth, J.A., and Moriera, W., "Deployment of the Hobby-Eberly Telescope Wide Field Upgrade", Proc. SPIE, 9145-5 (2014)

[8] Good, J.M., Hill, G.J., Leck, R.L., Landriau, M., Drory, N., Fowler, J.R., Kriel, H., Cornell, M.E., Booth, J.A., Lee, H., and Savage, R., "Laboratory Performance Testing, Installation, and Commissioning of the Wide Field Upgrade Tracker for the Hobby-Eberly Telescope", Proc. SPIE, 9145-156 (2014)
[9] Bacon, R., Accardo, M., Adjali, L., Anwand, H., Bauer, S., *et al.*, "The second-generation VLT instrument MUSE", Proc. SPIE 7735, 773508 (2010)
[10] Hill, G.J., "Replicated spectrographs in astronomy", Advanced Optical Technologies. Vol 3, Issue 3, 265 (2014)
[11] Hill, G.J., Gebhardt, K., Komatsu, E., Drory, N., MacQueen, P.J., Adams, J.A., Blanc, G.A., Koehler, R., Rafal, Roth, M.M., Kelz, A., Grupp, F., Murphy, J., Palunas, P., Gronwall, C., Ciardullo, R., Bender, R., Hopp, U., and Schneider, D.P., "The Hobby-Eberly Telescope Dark Energy Experiment (HETDEX): Description and Early Pilot Survey Results", ASP Conf. Series, 399, 115 (2008)
[12] Booth, J.A., Wolf, M.J., Fowler, J.R., Adams, M.T., Good, J.M., Kelton, P.W., Barker, E.S., Palunas, P., Bash, F.N., Ramsey, L.W., Hill, G.J., MacQueen, P.J., Cornell, M.E., and Robinson, E.L., "The Hobby-Eberly Telescope Completion Project", Proc SPIE 4837, 919 (2003)
[13] Booth, J.A., MacQueen, P.J., Good, J.G., Wesley, G.L., Segura, P.R., Palunas, P., Hill, G.J., and Calder, R.E., "The Wide Field Upgrade for the Hobby-Eberly Telescope", Proc. SPIE, 6267-97 (2006)
[14] Hill, G.J., MacQueen, P.J., Palunas, P., Barnes, S.I., and Shetrone, M.D., "Present and future instrumentation for the Hobby-Eberly Telescope", Proc. SPIE, 7014-5 (2008)
[15] Buckley, D.A.H., Swart, G.P., and Meiring, J.G., "Completion of the Southern African Large Telescope", Proc. SPIE, 6267-19 (2006)
[16] Burge, J.H., Benjamin, S.D., Dubin, M.B., Manuel, S.M., Novak, M.J., Oh, C.J., Valente, M.J., Zhao, C., Booth, J.A., Good, J.M., Hill, G.J., Lee, H., MacQueen, P.J., Rafal, M.D., Savage, R.D., Smith, M.P., and Vattiat, B.L., "Development of a wide-field spherical aberration corrector for the Hobby Eberly Telescope", Proc. SPIE, 7733-51 (2010)
[17] Oh, C.-J., Frater, E., Zhao, C., Burge, J.H., "System alignment and performance test of a wide field corrector for the Hobby-Eberly telescope", Proc. SPIE, 9145-8 (2014)
[18] Good, J., *et al*., "Design of performance verification testing for HET wide-field upgrade tracker in the laboratory," Proc. SPIE, 7739-152 (2010)
[19] Vattiat, B.L., *et al*., "Design, testing, and performance of the Hobby Eberly Telescope prime focus instrument package," Proc. SPIE, 8446-269 (2012)
[20] Vattiat, B.L., Hill, G.J., Lee, H., Moreira, W., Drory, N., Ramsey, J., Elliot, L., Landriau, M., Perry, D.M., Savage, R., Kriel, H., Haeuser, M., and Mangold, F., "Design, alignment, and deployment of the Hobby Eberly Telescope prime focus instrument package", Proc. SPIE, 9147-172 (2014)
[21] H. Lee, *et al.*, "Analysis of active alignment control of the Hobby-Eberly Telescope wide field corrector using Shack-Hartmann wavefront sensors," Proc. SPIE, 7738-18 (2010)
[22] H. Lee, *et al*., "Metrology systems for the active alignment control of the Hobby-Eberly Telescope wide-field upgrade," Proc. SPIE, 7739-28 (2010)
[23] H. Lee, *et al*., "Metrology systems of Hobby-Eberly Telescope wide field upgrade," Proc. SPIE, 8444-181 (2012)
[24] Adams, J.J., Uson, J., Hill, G.J., and MacQueen, P.J., "A new z = 0 metagalactic UV background limit," ApJ, 728, 107 (2011)
[25] Adams, J.J., Hill, G.J., and MacQueen, P.J., "B20902+34: a collapsing proto-giant elliptical galaxy at z=3.4", ApJ, 694, 314 (2009)
[26] Yoachim, P., *et al*.,, ApJ, 716, L4-8 (2010).
[27] Adams, J.J., *et al.*, "The Central Dark Matter Distribution of NGC 2976", ApJ, 745, 92 (2012)
[28] Adams, J.J., *et al*., "The HETDEX Pilot Survey I. Survey Design, Performance, and Catalog of Emission-Line Galaxies," ApJS, 192, 5 (2011)
[29] Blanc, G.A., et al., "The HETDEX Pilot Survey II: The Evolution of the Ly-α Escape Fraction from the UV Slope and Luminosity Function of 1.9<z<3.8 LAEs," ApJ, 736, 31 (2011)
[30] Finkelstein, S.L., *et al*., "The HETDEX Pilot Survey III: The Low Metallicities of High-Redshift Lyman Alpha Galaxies," ApJ, 729, 140 (2011)
[31] Song, M., Finkelstein, S.L., Gebhardt, K., Hill, G.J., Drory, N., Ashby, M.L.N., Blanc, G.A., Bridge, J., Chonis, T., Ciardullo, R., *et al*., "The HETDEX Pilot Survey V: The Physical Origin of Lyman-alpha Emitters Probed by Near-infrared Spectroscopy", ApJ, in press (arXiv:1406.4503) (2014)
[32] Tuttle, S.E., Hill, G.J., Lee, H., Vattiat, B.L., Noyola, E., Drory, N., Cornell, M.E., Peterson, T., Chonis, T.S., Allen, R.D., Dalton, G.B., DePoy, D.L., Edmonston, R.D., Fabricius, M.H., Kelz, A., Haynes, D.M., Landriau, M.,

Lesser, M.P., Leach, R.W., Marshall, J.L., Murphy, J.D., Perry, D., Prochaska, T., Ramsey, J., and Savage, R., "The construction, alignment, and installation of the VIRUS spectrograph", Proc. SPIE 9147-26 (2014)
[33] Marshall, J. L., DePoy, D. L., Prochaska, T., Allen, R. D., Williams, P., Rheault, J. P., Li, T., Nagasawa, D. Q., Akers, C., Baker, D., Boster, E., Campbell, C., Cook, E., Elder, A., Gary, A., Glover, J., James, M., Martin, E., Meador, W., Mondrik, N., Rodriguez-Patino, M., Villanueva, Jr., S., Hill, G. J., Tuttle, S., Vattiat, B., Lee, H., Chonis, T. S., Dalton, G. B., and Tacon, M., "VIRUS instrument collimator assembly," Proc. SPIE 9147-143 (2014)
[34] Kelz, A., Jahn, T., Haynes, D.M., Hill, G.J., Murphy, J.D., Rutowska, M., Streicher, O., Neumann, J., Nicklas, N., Sandin, C., Fabricius, M., and Tuttle, S.E., "HETDEX / VIRUS: testing and performance of 33,000 optical fibres", Proc. SPIE, 9147-269 (2014)
[35] H. Lee, et al., "VIRUS optical tolerance and production," Proc. SPIE, 7735-140 (2010)
[36] B. Vattiat, et al., "Mechanical design evolution of the VIRUS instrument for volume production and deployment," Proc. SPIE, 7735-264 (2010)
[37] Prochaska, T., *et al.*, "VIRUS spectrograph assembly and alignment procedures," Proc. SPIE, 8446-193 (2012)
[38] Tuttle, S.E., *et al*., "Initial results from VIRUS production spectrographs," Proc. SPIE, 8446-221 (2012)
[39] Adams, J.J., Hill, G.J., and MacQueen, P.J., "Volume phase holographic grating performance on the VIRUS-P instrument", Proc. SPIE, 7014, 701471 (2008)
[40] Chonis, T.S., Hill, G.J., Clemens, J.C., Dunlap, B., and Lee, H., "Methods for evaluating the performance of volume phase holographic gratings for the VIRUS spectrograph array," Proc. SPIE, 8446-209 (2012)
[41] Chonis, T. S., Frantz, A., Hill, G. J., Clemens, J. C., Lee, H., Adams, J. J., Marshall, J. L., DePoy, D. L., and Prochaska, T., "Mass production of volume phase holographic gratings for the VIRUS spectrograph array," Proc. SPIE 9151-53 (2014)
[42] Burgh, E.B., Bershady, M.A., Westfall, K.B., and Nordsieck, K.H., "Recombination Ghosts in Littrow Configuration: Implications for Spectrographs Using Volume Phase Holographic Gratings," PASP 119, 1069 (2007)
[43] Smith, M.P., Mulholland, G.T., Booth, J.A., Good, J.M., Hill, G.J., MacQueen, P.J., Rafal, M.D., Savage, R.D., and Vattiat, B.L., "The cryogenic system for the VIRUS array of spectrographs on the Hobby Eberly Telescope", Proc. SPIE, 7018-117 (2008)
[44] Chonis, T.S., *et al*., "Development of a cryogenic system for the VIRUS array of 150 spectrographs for the Hobby-Eberly Telescope," Proc. SPIE, 7735-265 (2010)
[45] Reiss, R., Deiries, S., Lizon, J.-L., and Rupprecht, G., "The MUSE instrument detector system", Proc. SPIE 8446, 84462P (2012)
[46] Snigula, J.M., *et al*., "Cure-WISE: HETDEX data reduction with Astro-WISE," Proc. SPIE, 8451-78 (2012)
[47] Snigula, J. M., Drory, N., Fabricius, M., Landriau, M., Montesano, F., Hill, G. J., Gebhardt, K., Cornell, M. E., "Cure-WISE: HETDEX Data Reduction with Astro-WISE", ASP Conf. Series, 485, 447 (2014)
[48] J.R. Tufts, P.J. McQueen, M.P. Smith, P.R. Segura, G.J. Hill, R.D. Edmonston, "VIRUS-P: camera design and performance", Proc. SPIE, 7021-10 (2008)
[49] Vattiat, B.V., *et al*., "Mechanical design evolution of the VIRUS instrument for volume production and deployment," Proc. SPIE, 7735-264 (2010)
[50] e.g. Allington-Smith J.R., *et. al*., "Integral Field Spectroscopy with the Gemini Multiobject Spectrograph. I. Design, Construction, and Testing", PASP, 114, 892 (2002)
[51] Barden S.C., and Wade, M.A., "DensePak and spectral imaging with fiber optics", in *Fiber optics in astronomy*; Proceedings of the Conference, Tucson, AZ, Apr. 11-14, 1988 (A90-20901 07-35). San Francisco, CA, Astronomical Society of the Pacific, 1988, p. 113-124
[52] Kelz, A., Bauer, S.M., Grupp, F., Hill, G.J., Popow, E., Palunas, P., Roth, M.M., MacQueen, P.J., and Tripphahn, U., "Prototype development of the integral-field unit for VIRUS", Proc. SPIE, 6273, 121 (2006)
[53] e.g. Schmoll, J., Roth, M.M., and Laux, U., "Statistical Test of Optical Fibers for Use in PMAS, the Potsdam Multi-Aperture Spectrophotometer," PASP, 115, 854 (2003)
[54] Murphy, J.D., Palunas, P., Grupp, F., McQueen, P.J., Hill, G.J., Kelz, A., and Roth, M.M., "Focal ratio degradation and transmission in VIRUS-P optical fibers", Proc. SPIE, 7018-104 (2008)
[55] Murphy, J.D., *et al*., "The Effects of Motion and Stress on Optical Fibers", Proc. SPIE, 8446-207 (2012)
[56] Lee, H., and Hill, G.J., "Image moment-based wavefront sensing for in-situ full-field image quality assessment," Proc. SPIE, 8450-191 (2012)

[57] Lee, H., Hill, G.J., Tuttle, S.E., and Vattiat, B.L., “Fine optical alignment correction of astronomical spectrographs via in-situ full-field moment-based wavefront sensing,” Proc. SPIE, 8450-192 (2012)
[58] Lee, H., Hill, G.J., Tuttle, S.E., Noyola, E., Peterson, T., and Vattiat, B.L., “Field application of moment-based wavefront sensing to in-situ alignment and image quality assessment of astronomical spectrographs: Results and analysis of aligning 100 VIRUS unit spectrograph,” Proc. SPIE, 9151-138 (2014).
[59] Chonis, T. S., Hill, G. J., Lee, H., Tuttle, S. E., and Vattiat, B. L., "LRS2: the new facility low resolution integral field spectrograph for the Hobby-Eberly Telescope," Proc. SPIE 9147-9 (2014)
[60] Prochaska, T., Allen, R., Rheault, J. P., Cook, E., Baker, D., DePoy, D. L., Marshall, J. L., Hill, G.J., and Perry, D., “VIRUS instrument enclosures,” Proc. SPIE 9147-257 (2014)
[61] Hill, G.J., Nicklas, H., MacQueen, P.J., Tejada de V., C., Cobos D., F. J., and Mitsch, W., "The Hobby-Eberly Telescope Low Resolution Spectrograph", Proc. SPIE, 3355, 375 (1998)
[62] Bershady, M.A., Andersen, D.R., Harker, J., Ramsey, L.W., and Verheijen, M.A.W., “SparsePak: A Formatted Fiber Field Unit for the WIYN Telescope Bench Spectrograph. I. Design, Construction, and Calibration”, PASP 116, 565 (2004)
[63] Bershady, M.A., “3D Spectroscopic Instrumentation” in ‘3D Spectroscopy in Astronomy, XVII Canary Island Winter School of Astrophysics’, Cambridge University Press, Cambridge, (2009)
[64] Le Fèvre, O., Maccagni, D., Paltani, S., Hill, L., Le Mignant, D., *et al*., “DIORAMAS: a wide-field visible and near-infrared imaging multi-slit spectrograph for the EELT”, Proc. SPIE 7735, 773528 (2010)
[65] Bigelow, B.C., Radovan, M.V., Bernstein, R., Onaka, P.M., Yamada, H., Isani, S., Miyazaki, S., and Ozaki, S., “Conceptual design of the MOBIE imaging spectrograph for TMT”, Proc. SPIE 9147-80 (2014)
[66] DePoy, D.L., Allen, R., Li, T., Marshall, J.L., Papovich, C., Prochaska, T., and Shectman, S., “An update on the wide field, multi-object, moderate-resolution, spectrograph for the Giant Magellan Telescope”, Proc. SPIE 9147-72 (2014)
[67] Lawrence, J.S., Brown, D.M., Brzeski, J., Case, S., Colless, M., Farrell, T.J., Gers, L., Gilbert, J., Goodwin, M, Jacoby, G., Hopkins, A.M., Ireland, M.J., Kuehn, K., Lorente, N.P.F., Miziarski, S., Muller, R., Nichani, V., Rakman, A., Richards, S., Saunders, W., Staszak, N.F., Tims, J., Vuong, M., Waller, L.G., “The MANIFEST fibre positioning system for the Giant Magellan Telescope”, Proc. SPIE 9147-341 (2014)